Subsea-to-surface Oil Transport in an Ambient Pressure Seawater Duct

Applied fluid dynamics of a buoyancy guide for oil spill recovery

Mike H. Wofsey[1], Richard Tipping[2],

1. CNJV, Contract to the U.S. Department of Energy, Golden Field Office, USA

2. University of Alabama, USA

[*1]michael.wofsey@go.doe.gov; [2]rtipping@ua.edu

Abstract

An applied fluid dynamics analysis is presented of oil droplets rising through an ambient-pressure subsea pipe or duct, which we describe as a buoyancy guide. This is applied to a novel method of subsea oil spill recovery from a broken subsea choke under ambient pressure at depth. We use a conventional Newtonian analysis to provide a first approximation of the buoyancy of oil droplets through this guide. We optimize a configuration with respect to the fluid dynamics of this system in order to optimise the mass transport of the oil droplets, and then propose a sample application. We find that a collection of narrower ducts is more efficient than one wide duct to deliver droplets of oil to the surface under their own buoyancy.

Introduction

Drilled petroleum products are typically transported from subsea wells by a pressurized piping system. In rare cases, due to an accident recovery process or due to environmental controls, oil may be mixed with water, which may prevent a high-pressure recovery. In these cases, we examine a first approximation of a method to concentrate the oil through natural buoyancy separation from depth. We find that careful attention should be given to the natural fluid dynamics of the system and the design of the duct in the particular. This research suggests that a deepwater ambient pressure recovery system is feasible.

Theory

The Relationship Between Droplet and Flow

We start with a single drop of oil of arbitrary size. Creating a force balance on the oil droplet, we have the buoyant force F_B acting upward on the oil droplet, and both the gravity force F_g and the viscous drag force F_D acting downward on the droplet. Applying this force balance,

$$F_B - (F_g + F_D) = m\frac{dv}{dt}, \qquad (1)$$

where v is the velocity of the oil droplet.

We note here that the oil rises though the water in the duct due to the buoyancy force alone. In a typical broken choke there will likely be a significant volume of released gas bubbles with the oil and water, but due to the relatively low Stokes velocity of the oil droplets, these will not impart significant additional speed to the system and should be removed through the sides of the pinhole scored duct so that turbulence is minimized.

Since $F_B = V_{oil}\rho_{water}g$, and $F_g = V_{oil}\rho_{oil}g$, and $F_D = 6\pi\eta Rv$, where V is the volume, ρ is the density, g is the acceleration due to gravity, η is the dynamic viscosity of the seawater, and R is the oil droplets Stoke's radius. This leads to,

$$V_{oil}\rho_{water}g - (V_{oil}\rho_{oil}g + 6\pi\eta Rv) = V_{oil}\rho_{oil}\frac{dv}{dt}. \qquad (2)$$

We divide both sides by the mass of the oil. The

terminal velocity of the oil droplet is low enough that we can neglect the very small time to acceleration of the droplet up to terminal velocity, so that $dv/dt = 0$, thus …

$$g\left(\frac{\rho_{water}}{\rho_{oil}}-1\right)-\frac{9\eta v_{term}}{2R^2\rho_{oil}}=0. \qquad (3)$$

Solving for v_{term},

$$v_{term}=\frac{2g\rho_{oil}R^2}{9\eta}\left(\frac{\rho_{water}}{\rho_{oil}}-1\right). \qquad (4)$$

Now, using the kinematics of the droplet, with the depth l of the oil source below the surface, we find

$$t=\frac{l}{v_{term}}=\frac{9\eta l}{2g\rho_{oil}R^2\left(\frac{\rho_{water}}{\rho_{oil}}-1\right)}, \qquad (5)$$

which is the theoretical, first approximation of time t that a droplet of Stokes radius R requires to reach sea level. This transport time is highly dependent on the Stokes radius R of the oil droplets. For the smallest droplets of about 10 μm in diameter, it will take approximately 37,000 hours to rise to sea level. But only a small number of oil droplets at the exit of a choke are typically this small. Rather, studies have shown the smallest range at the exit of a choke is in the 10 μm –15 μm range. Further downstream from the choke, the droplets coalesce and are in the range of 100 μm –200 μm. [1] The distribution of oil droplet sizes has also been studied experimentally in a wave tank. [2] Bubbles of density lower than the liquid layer were also studied and then fit to a modified Navier-Stokes equation. [3] Our work differs in that we are mostly interested in the kinematics of individual droplet movements as a means of separating the oil-water mixture. Conversely, a study was performed where turbulence was used to separate different density particles [4], however we examine only the laminar domain and examine the concentration of particles. The buoyancy of crude oil droplets in aqueous solutions was studied experimentally under low Reynolds number using capillary tubing, [5] this work approaches some of the same goals, but with Reynolds numbers closer to transitional.

The Relationship Between Duct and Flow

The flow $f = v_{term}A$, where A is the cross-sectional area of the duct, d is the diameter of the duct, and S is our Reynold's number, using the definition of Reynold's number this relation produces,

$$S=\frac{\rho_{water}v_{term}d}{\eta}=\frac{4\rho_{water}f}{\pi\eta d}. \qquad (6)$$

Solving this equation for f and using Eq. 4 along with $f = v_{term}A$,

$$\frac{S\pi\eta d}{4\rho_{water}}=\frac{2g\rho_{oil}R^2}{9\eta}\left(\frac{\rho_{water}}{\rho_{oil}}-1\right)\pi\left(\frac{d}{2}\right)^2, \qquad (7)$$

solving for d and simplifying,

$$d=\frac{9\eta^2}{2g\rho_{water}(\rho_{water}-\rho_{oil})}SR^{-2}. \qquad (8)$$

This gives the necessary duct diameter for an average Stokes radius R of oil droplets coming from a choke in order to keep the flow nonturbulent and allow the greatest coalescing between droplets to occur which will decrease travel time to the surface.

Application

A typical application where this may be useful would be a broken well choke at considerable depth below the surface, where the spilled oil would preferably be recovered at the surface in a floating boom corral after being delivered by the described deep sea ambient pressure duct. We use an average crude oil mass density of 875 kg/m³ and an average seawater mass density of 1,100 kg/m³, with g = 9.8m/s² , $\eta = 1.08\times10^{-3}P_a\cdot s$, using Eq. 5, we find that,

$$t\simeq(2.20\times10^{-6}m\cdot s)lR^{-2}. \qquad (9)$$

Using a droplet with Stokes diameter 200μm (a reasonable coalesced Stokes diameter some distance from the broken choke) at a depth of 1,500 m, we convert to Stokes radius with Eq. 9, and find that a droplet of that size would take about 92 hours to rise to the surface from the choke. If the droplet coalesces with other droplets (which is possible in a buoyancy guide under engineered conditions) then this time will decrease. For instance, if the average Stokes diameter became 500μm, the average time to the surface would fall to about 15 hours.

Using Eq. 8, we find that,

$$d\simeq(2.16\times10^{-12}m^3)SR^{-2}. \qquad (10)$$

Using a Reynold's number of S=4,000 which provides for a nonturbulent flow of the oil up through the duct, with an average Stokes diameter of 200μm, we find that the optimum diameter for each duct in the bundle would be about 86 cm. If the duct diameter becomes much larger than this, for this average droplet size,

then the system risks turbulence, which can break up oil droplets, making them smaller which will take them longer to get to sea level. So a collection of narrower ducts is apparently more efficient than one large duct.

We can use the constraint of duct diameter to help design the bundle of ducts. A given volume of oil W per period t emanating from the broken choke, could be distributed through a bundle of ducts so that,

$$W = \frac{N}{(\alpha+1)} \frac{\pi d^2 l}{4}, \qquad (11)$$

where N is the number of ducts in the bundle, α is a dilution value. For instance if the total volume of water plus oil contained in the duct has 5 parts seawater to 1 part crude oil, with 4,000m³/92 hours crude from the choke, then $\alpha = 5$, and the total

$$N = \frac{4W(\alpha+1)}{\pi d^2 l} \simeq 28 \text{ ducts.} \qquad (12)$$

Thus in this example, we will need a bundle of 28 ducts in parallel, each 86 cm diameter, to handle the flow and deliver the oil to the surface within the requisite constraints.

Engineering Design

Although the theory would change slightly due to the work required to lower the entropy of the oil-water system, this theory could be applied to larger oil sources, if the ducts are made from pin-scored flexible material of engineered pinhole diameter. This could potentially allow the coalesced oil to gradually concentrate in the duct as the water (with a lower surface tension) is gradually driven out of the sides of the duct.

The ducts could maintain rigidity by including flow-transverse seamed pole-pockets, which can be fitted with buoyant foam rings approximately every 2 to 10 meters in depth. The easiest way to accomplish this in our opinion is to use readily available flexible polyethylene, since the material comes in wide rolls, in lengths exceeding 30 meters. Further, the material can be readily treated with mechanical scoring to produce micron-sized perforations (in a stochastic pattern so the material won't be weakened), which will produce the requisite semi-permeable effect. Alternatively, prescored material may be available from the use of oil-absorbent booms. This material can be quickly seamed with existing microwave seaming systems.

Industry-standard 5-foot-wide rolls of material can be seamed into the 0.1 to 0.48 m diameter ducts. Including the pockets for the closed-cell foam floatation (the deeper portions of the duct will require density-adjusted closed-cell foam), a typical on demand emergency module would need approximately 4,000 of these 5-foot by 100-foot rolls. A possible incarnation of this effect can be seen in Figure 1. *Please note that in this figure, the box simply provides a structure to attach the ducts and direct the oilwater mixture into the ducts. No separation of the oil-water mixture takes place in the box, the separation of the oilwater mixture happens as it gradually rises through the ducts, due to the low buoyancy of the oil relative to the water through which it moves as shown in the previous calculations. High turbulence is expected inside of the box due to the impact of the oil with the water as it leaves the broken choke, which will cause atomisation of the oil droplets.*
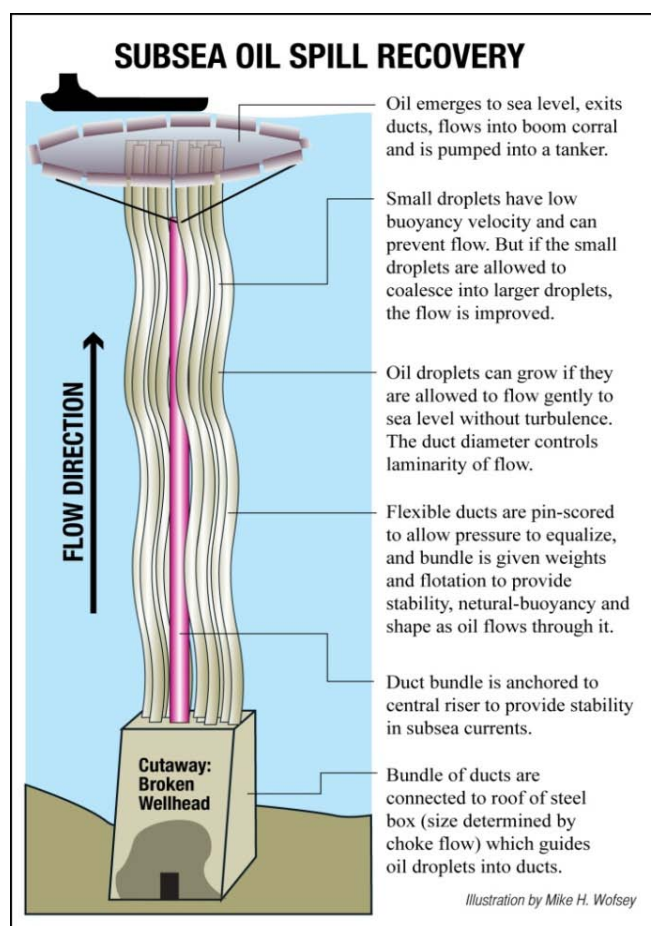

FIG. 1 SUGGESTED APPLICATION OF OIL BUOYANCY GUIDE

The finished box would be lowered over the broken wellhead, with the ducts streaming up, and set into position around the simultaneously descending stabilization rod. Since there is little pressure introduced to the flow above ambient conditions, there should not be a problem with crystallization at the choke, and the flow should rise upward as if it is

unconstrained by the duct, to the surface, into a boom corral, where the surface oil will be pumped aboard a tanker.

The oil that emerges from the choke is quickly atomized on contact with the water due to the essentially high Reynold's number of unguided flow, which significantly increases turbulence. These tiny droplets quickly decelerate on contact with the water, because the natural Stokes velocity of oil droplets this small is low. The necessary volume of the box is determined by the volume of oil coming from the broken choke per unit time and is likely determined experimentally. This remains for future research.

Strengthening Duct System Due to Near-surface Ocean Currents

The properly constructed boom will can experience current near the surface which should offer additional extension greater than l, for instance at a depth of 1,500 m,

$$l^{'} = \frac{2l}{\sqrt{2}} \simeq 2,121 \text{m}. \qquad (2.18)$$

This is determined by assuming a 45° angle to the horizontal of the duct. This will lower the force exerted on the duct per unit of vertical rise, from subsea currents. While the ducts are flexible, they are at neutral pressure with the surrounding water and area anchored to a central riser. We expect this to provide the necessary stability against upper-layer ocean currents in excess of 1 m/s, the design specifics will require further experimentation.

Conclusion

As shown in previous subsea spills, there are few viable ways of quickly capturing oil spills at a broken choke, due to the high pressure at the choke and high pressure at depth. As shown in this analysis, the fluid dynamics of capturing released oil will require careful attention to guide the oil droplets up to the surface in a way that encourages coalescence rather than encourages atomisation. The latter will result in a total mass of oil that will take a significantly longer time to surface and may present a barrier that won't allow new oil up the duct. The system described in this paper would likely be made as an emergency device ahead of time with the collapsible ducts stored on top of the unit, and then lowered to the broken choke when needed. We believe that the strength of this proposal is

in the speed to implement and the relative safety in protecting the damaged choke.

REFERENCE

Eric Climent and Jacques Magnaudet "Large-Scale Simulations of Bubble-Induced Convection in a Liquid Layer" Phys. Rev. Lett. 82, 4827–4830 (1999).

Enrico Calzavarini, Massimo Cencini, Detlef Lohse, and Federico Toschi "Quantifying Turbulence-Induced Segregation of Inertial Particles" Phys. Rev. Lett. 101, 084504 (2008).

Eisa AlMatroushi and Mamdouh T. Ghannam, "Buoyancy Driven Motion of Crude Oil Droplet within Aqueous Solutions." IJET-IJENS Vol: 12, No: 03 (2012).

M.J. van der Zande, P.H. Janssen, W.M.G.T. van den Broek, "Size of oil droplets under high-water-cut conditions" SPE Production and Operations Symposium, (2001).

Zhengkai Li, Kenneth Lee, Thomas King, Michel C. Boufadel, and Albert D. Venosa "Oil droplet size distribution as a function of energy dissipation rate in an experimental wave tank" International Oil Spill Conference Proceedings: May 2008, Vol. 2008, No. 1, pp. 621-626. (2008).

Mike H. Wofsey is from Denver, Colorado. He received his Ph.D. in applied physics from the University of Alabama, in Tuscaloosa, Alabama, USA, in 2010.

He is a Senior Engineer with CNJV, contract to the U.S. Department of Energy, Golden Field Office, Golden, Colorado. He pursues work in ion-polarization and particulate aggregation. He is author of U.S. Patents in

desalination and ion-polarization.

Dr. Wofsey continues to serve as scientific consult for humanitarian desalination water projects in Developing Nations.

Richard Tipping received his doctoral degree from The Pennsylvania State University in 1969.

He is Professor Emeritus for The University of Alabama, Tuscaloosa, Alabama and pursues research in the areas of theoretical molecular spectroscopy and collision-induced absorption and light scattering with applications to atmospheric physics.

Studies on Ethanol Gas Sensing Properties of Al$_2$O$_3$-doped ZnO Thick Films

M. K. Deore[1]*, G. H. Jain[2]

[1]Arts, Science and Commerce College, Ozar (Mig)-422 206, India

[2] Head, Dept. of Physics, K. T. H. M. College, Nashik, India

* Corresponding author: deoremadhav@rediffmail.com

Abstract

The thick films of undoped and Al$_2$O$_3$ - doped ZnO were prepared by screen printing technique. AR grade Zinc Oxide powder (99.9% pure) was mixed mechnochemically with different wt. %(0.5, 1 and 3) of Aluminium Chloride (Hexahydrate) (AlCl$_3$.6H$_2$O) in Acetone medium to obtain Al$_2$O$_3$ - ZnO composite material. The prepared materials were sintered at 1000°C for 12h in air ambience and reground to ensure sufficiently fine particle size. The electrical, structural and morphological properties of the films were investigated. The X-ray diffraction analysis of undoped and Al$_2$O$_3$ - doped ZnO material showed the polycrystalline nature. The surface morphology of the films was studied by SEM indicating that the films are granular and porous. The final composition of each film was determined by EDAX analysis. The gas response of undoped and doped ZnO films was studied for different gases such as CO, H$_2$, NH$_3$, and Ethanol at operating temperature ranging from 50°C to 450°C. The undoped ZnO film showed the poor response to Ethanol gas, while the film doped with 1 wt. % Al$_2$O$_3$ gave the good response to ethanol gas (500ppm) at 400°C. The selectivity, response and recovery time of the sensor were measured and presented.

Introduction

In recent years, the concern over environmental protection and increasing demands for monitoring hazardous and inflammable gases in industry and home have attracted extensive interests in developing gas sensors for these gases. Due to the advantages of small size, low cost, simple operation and good reversibility, the semiconductor sensors have become the most promising devices among the solid-state chemical sensors. Many semiconductor oxides such as ZnO, SnO$_2$, TiO$_2$, Cr$_2$O$_3$, Fe$_2$O$_3$, In$_2$O$_3$, CeO$_2$, WO$_3$, and CuO, have been explored to detect the toxic and inflammable gases, such as CO, CO$_2$, NO$_X$, H$_2$S, LPG and ethanol.

In order to enhance the catalytic activity (oxidation), the oxides were doped with it using mechanical mixing of some impurities. The aim of the present research work is to enhance the catalytic activity (oxidation) of Zinc Oxide (ZnO) using mechanical mixing of Al$_2$O$_3$ which is weak n-type semiconductor material with wide band gap (8.8 ev) for bulk material in different crystalline form and good thermal stabilit, and works as good catalyst with semiconductor when the gases such as H$_2$S and Ethanol come in contact with. The conventional oxide-mixing techniques; powders are produced more homogeneous after the sintering process.

Zinc Oxide is a wide band gap semiconductor with a bandgap of 3.37 eV and a large binding energy of 60 meV. It is an important semiconductor material, having a wide range of applications such as, luminescent devices, solar cells, chemical sensors etc, whose conductivity can be tailored by controlling the deviation from stoichiometry and by doping. Appropriate doping can provide electronic defects that increase the influence of oxygen partial pressure on the conductivity. In this work, Al^{3+} substitution on Zn^{2+}(was chosen due to the small ion size of Al^{3+} compared to that of Zn^{2+}(Al^{3+} (0.53Å) and Zn^{2+} (0.74 Å).

Ethanol is a hypnotic (sleep producer) gas having toxic nature. Heavy exposure and-/or consumption of alcoholic beverages, particularly by smokers, increase the risk of cancer of the upper respiratory and digestive tracks. Among women, the chances of breast

cancer increase with alcoholic consumption or exposure. Those working on ethanol synthesis have great chances of being victims of respiratory and digestive track cancer. So there is a great demand and emerging challenges for monitoring ethanol gas at trace level.

Experimental procedure

Preparation of Functional Material

AR grade Zinc Oxide powder (99.9% pure) was sintered at 1000^0C for 12 h. The sintered Zinc Oxide powder (99.9% purity) was mixed mechnochemically with different wt. %(0.5, 1 and 3) of Aluminium Chloride (Hexahydrate) ($AlCl_3.6H_2O$) in Acetone medium to obtain Al_2O_3 - ZnO composite materials. The prepared composite materials were sintered at 1000°C for 12h in air ambience and reground to ensure sufficiently fine particle size.

Preparation of Thick Films

The thixotropic paste was formulated by mixing the fine powder of functional material with ethyl cellulose (a temporary binder) in an organic solvent such as butyl cellulose, butyl carbitol acetate and terpineol etc. The ratio of the inorganic to organic part was kept at 75:25 (Volume) in formulating the paste. This paste was screen-printed on a glass substrate in a desired pattern (1.5 cm X 0.5 cm). The films were dried under infrared radiation for 45 minutes. To remove the organic vehicle, the films were fired at a temperature of 550°C for 30 min then attained at room temperature in a muffle furnace.

Thickness Measurements

The range of thicknesses of the films was observed from 65 to 75 μm. The reproducibility in thickness of the films was possible by maintaining the proper rheology and thixotropy of the paste.

Physical Characterization

Structural Analysis

In order to understand the structural properties of Al_2O_3 - doped ZnO composite powder materials at different dopant concentration, X-ray diffraction analysis of these sintered powders was carried out in the 20-80^0 range using Cuk$_\alpha$ radiation.

Fig.1 shows XRD patterns of undoped- ZnO and Al_2O_3 (0.5, 1 and 3 wt. %) – doped ZnO.

Fig.1 (a) shows XRD patterns of undoped ZnO material. The observed diffraction peaks are corresponding to the hexagonal wurtzite structure of ZnO and well matched with the JCPDS (76-0704) reported data of ZnO. The sharp peaks of XRD were attributed to ZnO material observed to be polycrystalline in nature. The higher peak intensities of an XRD pattern is due to the better crystallinity with preferred orientation along the (101) direction.
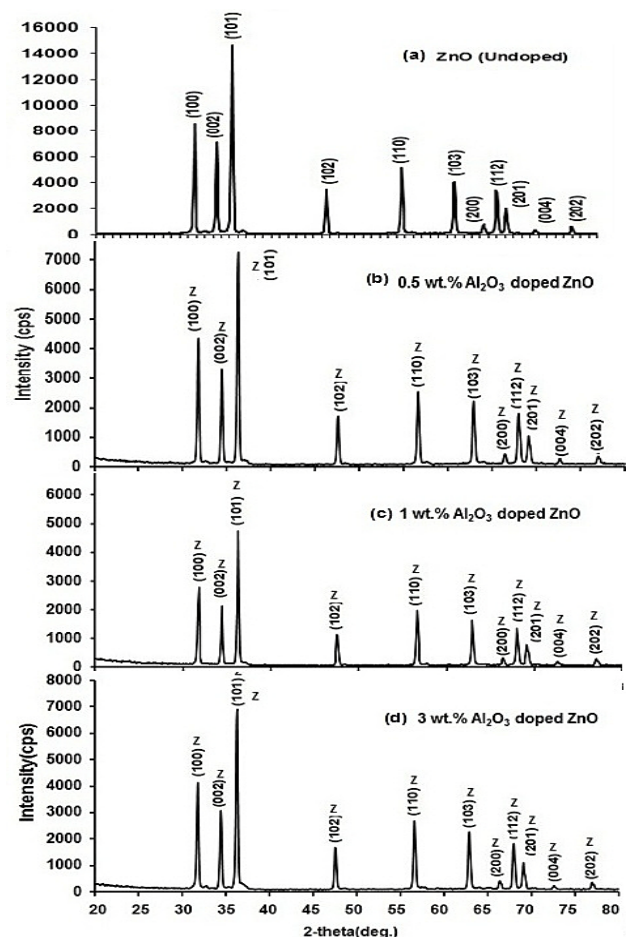

FIG. 1 XRD PATTERN FOR Al_2O_3 –DOPED ZnO COMPOSITE MATERIAL

Figs. 1(b - d) shows the XRD patterns of Al_2O_3 (0.5, 1 and 3wt. %) – ZnO composite material. For all compositions, formation of only ZnO wurtzite phase is observed in accordance with the reported d-values (JCPDS 76-0704). The possible formation of Al_2O_3 or $ZnAl_2O_4$ phases was not detected. This might be due to relatively low sintering temperature (~1000°C) at which Al into Zn sites might not have occurred to a complete extent.

From the XRD results, it is concluded that the material properties are strongly dependent on Al_2O_3 concentration. The 1 wt. % of Al_2O_3 doping is critical to have high quality ZnO material. Moreover, the (002)

diffraction peak intensity of ZnO: Al_2O_3 decreases. This indicates that the doping concentration deteriorates the crystallinity of the material, which may be due to the formation of the stresses by the difference in ion sizes between Zinc and the dopant and the segregation of dopants around grain boundaries at high doping concentrations.

The average crystallite size was calculated from XRD pattern using Debye Scherer's formula.

$$D = 0.9\lambda / \beta Cos\theta \qquad (1)$$

Where D- Average crystallite size, β - Broadening of the diffraction line measured at half maximum intensity (FWHM), λ -Wavelength of the x- ray radiation and θ -Bragg's angle.

The crystallite size for undoped ZnO lies in between 27-36 nm while Al_2O_3 - doped ZnO lies in between 10-36 nm. Thus the crystallite size varies with doping concentration of Al_2O_3 in ZnO samples. Slightly broadening of diffraction lines may be attributed to small crystalline effects.

Micro Structural Analysis of the Films

The surface morphology and chemical composition of the films were analyzed using a scanning electron microscope [SEM model JEOL 6300 (LA) Germany] coupled with an energy dispersive X-ray analysis. (EDAX, JEOL, JED-2300, Germany).

SEM images in Fig. 2 show the surface morphology of undoped ZnO and Al_2O_3 (0.5, 1 and 3 wt. %) – doped ZnO thick films. Fig. 2 (a) shows the micrograph of pure ZnO thick film. It consists of randomly distributed particles with smaller size and shape and with limited porosity. The particle size of films varies in between 186 nm to 190 nm. Plane-view SEM investigation of Fig.2 (b-d) reveals a porous structure of Al_2O_3 doped - ZnO thick films. Petal-shaped particles of various sizes (156-225 nm) were observed in all samples. The majority of these particles appear several times larger than the average crystallite sizes calculated from X-ray diffraction data (10-36 nm) thus, indicating that most of the particles comprise multiple crystallites. No systematic variation in the microstructure of the ZnO films as a function of the doping concentration was observed.

In Fig.2 (b), the Al_2O_3 additives distributed on ZnO grains would be very less, so they are not sufficient to accelerate the sensing reaction with the target gas, hence it shows the poor response to the target gas.

In Fig. 2(c), the Al_2O_3 additives present on the ZnO

grains are at an optimum level leading to high porosity and large effective surface area available for the adsorption of oxygen species. The ZnO film doped with 1 wt. % Al_2O_3 was observed to be the most sensitive to ethanol than the other films.

In Fig.2 (d), Al_2O_3 particles present over ZnO surface would be greater than optimum level, Which reduces the porosity and resists reaching the target gas to the inter-grain boundary of Al_2O_3 –ZnO, hence the film shows poor response to ethanol gas.
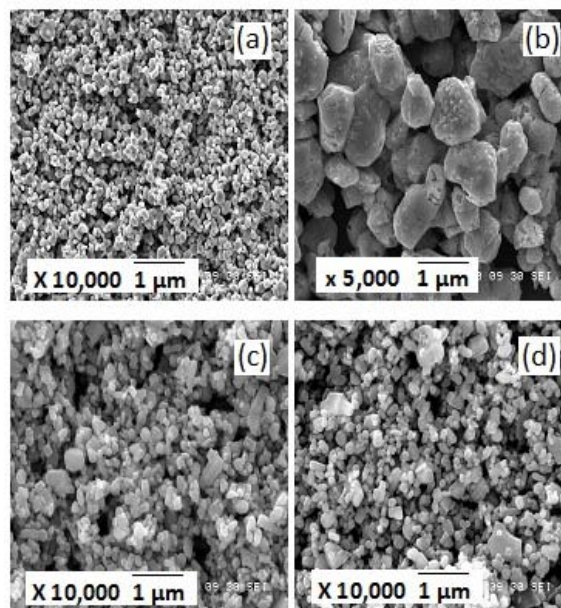

FIG. 2 SEM IMAGES OF (a) UNDOPED ZnO, (b) 0.5 wt.% (c)1 wt.% AND (d) 3 wt.% Al_2O_3 – ZnO FILMS

The specific surface area was determined by the equation (2).

$$S = \frac{6}{\rho * D} \qquad (2)$$

Where S is specific surface area, ρ is density of material and D is diameter of particle. The specific surface area of the films is shown in Table 1.

TABLE 1 PARTICLE SIZE AND SPECIFIC SURFACE AREA OF Al_2O_3 -DOPED ZNO FILMS.

Sr. No.	Wt. % of Al_2O_3	Particle size (nm)	Specific Surface Area(m^2/gm)
1	Pure ZnO	186	5.75
2	0.5	156	34.60
3	1	195	27.91
4	3	225	25.00

Elemental Analysis of the Films

The composition of undoped and Al_2O_3 -doped ZnO thick films was analyzed by energy dispersive X-ray analysis.

TABLE 2 QUANTATIVE ELEMENTAL ANALYSIS OF UNDOPED AND AL₂O₃ -DOPED ZNO FILMS.

Elements	ZnO (undoped)	Doping level(Al₂O₃- ZnO)		
		0.5 wt. %	1wt. %	3 wt.%
O (mass %)	19.66	19.78	20.07	20.16
Zn (mass %)	80.34	79.99	79.14	78.87
Al (mass %)	--	0.23	0.79	0.97
Total	100	100	100	100

Table.2 gives quantitative elemental analysis of undoped and Al₂O₃ -doped ZnO thick films at different doping concentration. The EDAX analysis shows presence of only Zn, Al and O as expected, no other impurity elements were present in the thick films. The EDAX result shows variation in Zn/O ratio and Al/Zn ratio with variation in doping concentration. The mass percentage(%) of Zn and O in each sample was not as per stoichiometric proportion. The entire samples were observed to be oxygen deficient that would promote the adsorption of relatively large amount of oxygen species favorable for higher gas response. It suggests the role of Al as one of the either providing additional adsorption sites for the reaction or stabilizing the sites already existing on the ZnO surface. The stabilizing action of Al ions can be visualized as the localization of the free electron of Zinc into ZnO by overlapping them with their own electron clouds.

Electrical Conductivity of the Films

Fig.3 shows the variation of log (conductivity) with reciprocal of temperature of undoped and Al₂O₃-doped ZnO films. It is clear from graph that the conductivity of these films goes on increasing with increase in temperature, indicating negative temperature coefficient (NTC) of resistance. This shows that the materials are semiconducting nature.
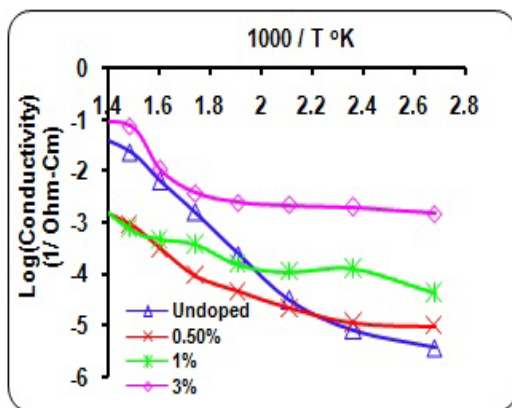

FIG.3 CONDUCTIVITY- TEMPERATURE PROFILE OF UNDOPED AND Al₂O₃ - DOPED ZnO FILMS

Fig.3 shows that the conductivity of films increases with increase in dopant concentration of Al₂O₃.. Thus, it was found that the conductivity of Al₂O₃- ZnO films is strongly dependent on the Al₂O₃ dopant concentration.

Gas Sensing Performance

The gas sensing performance of undoped and Al₂O₃-doped ZnO thick films was studied by using static gas sensing system. The conductance of thick films was measured as a function of temperature in air as well as in CO, H₂, NH₃, and Ethanol gases atmosphere. The operating temperature was varied from 50°C to 450°C. From the measured conductance in air as well as in gases atmosphere, the gas response was determined at particular operating temperature using the equation (3).

$$S = \frac{(G_{gas} - G_{air})}{G_{air}} \qquad (3)$$

Where G_{air} = conductance of thick film in air.

G_{gas} = Conductance of thick film in gas.

Fig. 4 shows the variation in the gases response of 1wt. % Al₂O₃ -doped ZnO film for the gases viz: CO, H₂, NH₃ and ethanol as the function of operating temperatures. The doped film shows the highest response to Ethanol gas (500 ppm) at 400°C. The response goes on increasing with increase in operating temperature, attains its maximum (at 400°C) and then decreases with a further increase in operating temperature. It is clear from the graph that the optimum operating temperature is 400°C for ethanol gas.
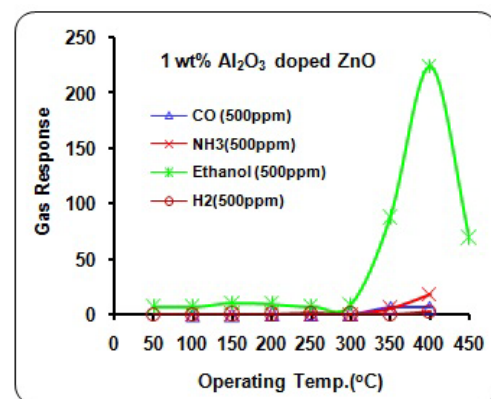

FIG. 4 VARIATION IN GAS RESPONSE WITH OPERATING TEMPERATURE OF 1 wt. % Al₂O₃ –DOPED ZnO FILM

Fig.5 shows the variation in Ethanol gas sensing performances of undoped- ZnO and Al₂O₃ doped-ZnO thick films at different doping concentration (0.5, 1 and 3 wt. %) as the function of operating

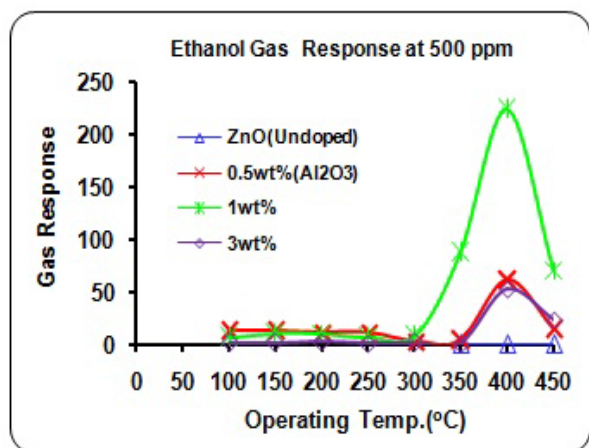temperatures ranging from 50°C to 450°C.

FIG. 5 VARIATION IN ETHANOL GAS RESPONSE WITH OPERATING TEPMERATUE OF UNDOPED AND Al₂O₃-DOPED ZnO FILMS

It was noted from the graph that the undoped ZnO thick film was observed to be poor response for Ethanol gas while all doped films showed the good response to Ethanol gas at 400 °C. The gas response increases with increase in temperature and then decreases with further increase in operating temperature. It has been observed that the increased gas response of thick film sensor is due to the dopants or additives which enhance the chemisorptions of the film to specific gases.

Selectivity of doped ZnO Film

The selectivity is the ability of a sensor to respond to certain gas in the presence of other gases. Percentage selectivity of one gas over the other is defined as the ratio of maximum response of other gas to the maximum response to the target gas at the optimum temperature.
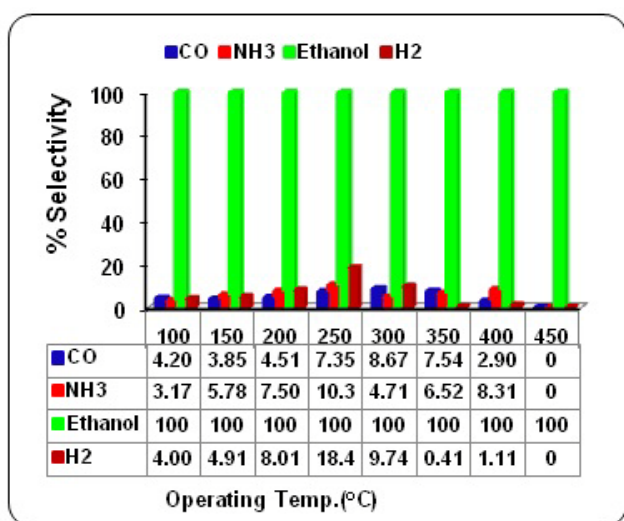

FIG. 6 % SELECTIVITY OF 1wt. % Al₂O₃ -DOPED ZnO FILM

The bar diagram in Fig. 6 indicates percentage selectivity of 1wt. % Al₂O₃ - doped ZnO thick film as a function of operating temperature for different gases. It is clear from the bar diagram that the doped thick film (1 wt. % Al₂O₃) is more selective to ethanol against the other gases viz: CO, NH₃, and H₂. This is the main feature of Al₂O₃ - ZnO thick film.

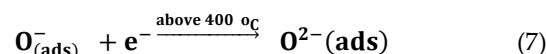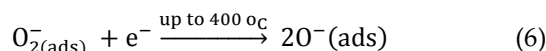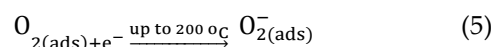### Response and Recovery Time of 1 wt. % Al2O3 -ZnO Film

Response time is the time taken for the sensor to attain 90% of the maximum increase in conductance on exposure to the target gas and recovery time is the time taken by the sensor to get back 90% of the original conductance.

The doped ZnO thick film was quick (~ 10 s) to Ethanol gas while the recovery was (~ 40 s). The quick response may be due to faster oxidation of gas. The aluminium species catalyses the reaction promoting the rapid electron transfers between the adsorbate and substrate.
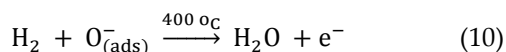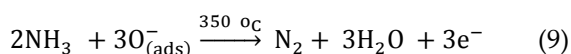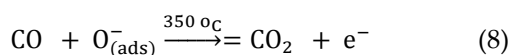
Discussion

Gas Sensing Mechanism Al2O3 -Doped ZnO Thick Film

The gas sensing mechanism of the metal oxide semiconductor sensors belong to the surface controlled type, which is based on the change in conductance of the semiconductor. The oxygen adsorbed on the surface directly influence the conductance of metal oxide based sensors. Oxygen is adsorbed on the oxide crystals surface as ions are formed by abstracting free electrons from the metal oxide semiconductors, reducing the electrical conductivity. The amount of oxygen adsorbed on the sensor surface depends on operating temperature, concentration of additives, particle size, and specific surface area of the sensor. In the aerial atmosphere where the partial pressure of oxygen is taken as constant, oxygen is adsorbed on sensor surfaces of - Al₂O₃ –doped- n-type ZnO in the form of O, O₂⁻ and O²⁻ depending on the temperature, The state of oxygen on the surface of ZnO sensor undergoes the following reactions:

$$O_{2(gas)} \rightarrow O_{2(ads)} \quad (4)$$

$$O_{2(ads)+e^-} \xrightarrow{\text{up to } 200 \, ^oC} O_{2(ads)}^- \quad (5)$$

$$O_{2(ads)}^- + e^- \xrightarrow{\text{up to } 400 \, ^oC} 2O^-(ads) \quad (6)$$

$$O_{(ads)}^- + e^- \xrightarrow{\text{above } 400 \, ^oC} O^{2-}(ads) \quad (7)$$

The oxygen species capture electrons from the material, which results in the concentration changes of holes or electrons in the Al_2O_3 doped n-type ZnO semiconductor.

In the presences of gases viz: CO, H_2 and NH_3, the sensing mechanism at different temperatures could be expressed through the following reactions.

$$CO + O_{(ads)}^- \xrightarrow{350\ ^oC} = CO_2 + e^- \qquad (8)$$

$$2NH_3 + 3O_{(ads)}^- \xrightarrow{350\ ^oC} N_2 + 3H_2O + 3e^- \qquad (9)$$

$$H_2 + O_{(ads)}^- \xrightarrow{400\ ^oC} H_2O + e^- \qquad (10)$$

In the presences of Ethanol vapours, the reason for a decrease in the resistance may be due to the oxidation of the ethanol vapours upon coming in contact with the Al_2O_3:ZnO film surface, which liberates free electrons and H_2O. Ethanol vapours react with the chemisorbed oxygen and reject the carrier, thereby reducing the resistance of the Al_2O_3: ZnO material.

The possibility of a reaction of ethanol with the Al_2O_3: ZnO sensing layers can be explained as two oxidation states :

$$C_2H_5OH_{(g)} + [O] \rightarrow CH_3CHO + H_2 \qquad (11)$$
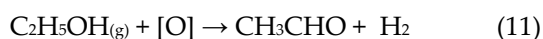
(The dehydrogenation to acetaldehyde

$$C_2H_5OH_{(g)} + [O] \rightarrow C_2H_4 + H_2O \qquad (12)$$
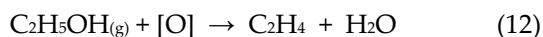
(The dehydration to ethylene)

Where [O] represents the surface oxygen ions.

The first reaction (11) is a process initiating the oxidation by the dehydrogenation to CH_3CHO intermediate, and the second reaction (12) is initiated by the dehydration to C_2H_4. But the selectivity for the two reactions is initiated by the acid–base properties of the oxide surface. The dehydrogenation process is more probable on the oxide surface with basic properties, while the dehydration is favoured on the acid surface.

Finally intermediate products, acetaldehyde and ethylene, are subsequently reduced to CO_2 and H_2O.

$$C_2H_5OH_{(g)} + 6O^{2-}_{(film\ surface)} \rightarrow 2CO_2 + 3H_2O + 12\ e^-_{(cond.\ band)}$$
$$(13)$$
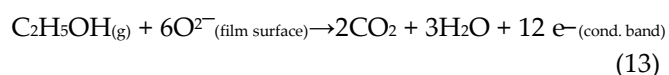
At higher temperature, the depletion region created by the chemisorptions of oxygen on the surface extends more deeply, providing larger scope for more gaseous elements to be adsorbed, thereby giving a better response. Also, the hydroxyl group desorbs at higher temperatures. Thus for lower temperature operation

(<150°C), the surface of the sensor does not get completely desorbed, which causes a smaller change in resistance. Thus Al_2O_3: ZnO composite has found to markedly and effectively promote the sensitivity to ethanol gas.

Summary and Conclusions

From the results obtained, following conclusions can be made for the sensing performance of the sensors.

i. The undoped ZnO thick film showed low response to ethanol gas.

ii. The 1 wt. % Al_2O_3 -doped ZnO thick showed good response to ethanol gas at 400°C.

iii. The 1wt. % Al_2O_3 -ZnO thick film has observed the most porous which showed maximum response to ethanol gas.

iv. The 1 wt. % Al_2O_3 -doped ZnO thick film sensor has good selectivity to ethanol against, CO, NH_3 and H_2 gas at temperatures.

v. The Al_2O_3 –doped ZnO thick film sensors showed very rapid response (~4s) and recovery (~40s) to ethanol gas.

vi. Over long exposure, it was observed that thick film exhibited a good stability and repeatability as gas sensor with consistent pattern and response magnitude. These studies showed that screen printed thick film of Al_2O_3 doped ZnO thick film on glass substrate can be used as ethanol gas sensor.

REFERENCES

Al-Kuhaili M. F., Durrani S. M. A., Bakhtiari I. A., "Carbon Monoxide gas –sensing properties of CeO2- ZnO thin films", Applied Surface Science, 255, 3033-3039, 2008.

Aranovich Julio, "Optical and electrical properties of ZnO films prepared by spray pyrolysis for solar cell applications", Journal of Vacuum Science and Technology, Vol.16, Issue: 4: 994-1003, 1979.

Arshak K., Gaidan I., "Gas sensing properties of

ZnFe$_2$O$_4$/ZnO screen-printed thick films", Sens. Actuators B 111–112, 58–62, 2005.

Bene R., Perczel I. V., Meyer F. A., Fleisher, Meixner M. H., "Chemical reactions in the detection of acetone and NO by a CeO$_2$ thin film", Sens. Actuators B: Chem.,71, 36–41,2000.

Chang J. F., Shen C. C., Hon M. H., "Growth characteristics and residual stress of RF magnetron sputtered ZnO:Al films", Ceramics International, Volume 29, Issue 3: 245–250 , 2003.

Cullity B. D., "Elements of X-ray diffraction", 2nd Edition (Addison Wesley) 1978.

Deore M. K., Gaikwad V. B., Patil N. U., Hire P. D., Chaudhari R. M., Wagh V. G., Jain G. H., "Formulation, Characterization and LPG-Sensing Properties of CuO-Doped ZnO Thick Film Resistor", Advancement in Sensing Technology', Smart Sensors, Measurement and Instrumentation, Springer Berlin Heidelberg, Vol. 1, 283-298,2013.

Gaikwad V. B., Deore M. K., Khanna P. K.,Kajale D. D., Shinde S. D., Chavan D. N., and Jain G. H., "Studies on Gas Sensing Performance of Pure and Nano- Ag Doped ZnO Thick Film Resistors", Recent Adv. in Sensing Technology, Springer-Verlag Berlin Heidelberg LNEE 209,49, 293–307, 2009.

Gregory J. Exarhos, Shiv K. Sharma, "Influence of processing variables on the structure and properties of ZnO films", Thin Solid Films 270, 27-32, 1995.

Islam M. R, Kumazawa N. Takeuchi M. "Chemical sensor based on titanium dioxide thick film:Enhancement of selectivity by surface coating", Appl. Surf. Sci., 142, 262-266, 1999.

Jagadish C., Pearton S., Zinc Oxide Bulk, "Thin films and nanostructures: Processing, Properties and applications", Elsevier limited, 2006.

Jain G. H., Patil L. A., Wagh M. S., Patil D. R., Patil S. A., Amalnerkar D. P., "Surface modified BaTiO$_3$ thick film resistors as H2S gas sensors", Sens. Actuators,117, 159–165,2006.

Jain G. H., Gaikwad V. B., Patil L. A., "Studies on gas sensing performance of(Ba0.8Sr0.2) (Sn$_{0.8}$Ti$_{0.2}$)O$_3$ thick film resistors", Sens. Actuators, 122, 605–612, 2007.

Kim S. R., Hong H. K., Kwon C. H., Yun D. H., Lee K., Sung Y. K., "Ozone sensing properties of In$_2$O$_3$-based semiconductor thick films", Sens. Actuators B: Chem, 66 , 59–62,2000.

Kohl D. "Surface processes in the detection of reducing gases with SnO2-based devices". Sens. Actuators B, 18, 71-113, 1989.

Lee E. T., Jang G. E., Kim C. K., Yoon D. H., "Fabrication and gas sensing properties of Fe$_2$O$_3$ thin film prepared by plasma enhanced chemical vapor deposition (PECVD)", Sens. Actuators B: Chem. 77, 221–227,2001.

Lupan O., Chai G., Chow L., "Novel hydrogen gas sensor based on single ZnO nanorod", Microelectron. Eng., Vol. 85, 2220–2225, 2008.

Mancic L., Marinkovic Z., Vulic P., Moral C. and Milosevic O.,"Nonstoichiometry of ZnCr$_2$O$_4$ nanophased powder", Sensors, 3, 415, 2003.

Matsushima S., Maekawa T., Tamaki J., Miura N., Yamazoe N.,"Role of Additives on Alcohol Sensing by Semiconductor Gas Sensor". Chem. Lett., 18, 845-848, 1989.

Morrison S. Roy, "Selecticvty in semiconductor gas sensors", Sens. Actuators, 12, 425-440, 1987.

Patil D. R. , Patil L. A., Jain G. H., Wagh M. S., Patil S. A., "Surface activated ZnO thick film resistors for LPG gas sensing", Sensors & Transducers, 74, 874- 663 ,2006.

Patil D. R., Patil L. A., "Cr$_2$O$_3$-modified ZnO thick film resistors as LPG sensors", Talanta 77, 1409–1414, 2009.

Raju A. R., Rao C. N. R., "Gas sensing characteristics of ZnO and copper impregnated. ZnO", Sens. Actuators B 3, 305–310, 1991.

Sahay P. P., Nath R. K., "Al-doped Zinc Oxide thin films for liquid petroleum gas (LPG) sensor", Sens. Actuators B, 133, 222-227, 2008.

Seeley Z. M., Bandyopadhyay A., Bose S., "Influence of crystallinity on CO gas sensing for TiO2 films", Materials Science and Engineering B 164 , 38–43,2009.

Singh, Shubra, Thiyagarajan P., Mohan Kant, K., D. Anita, Thirupathiah S ., Rama N., Tiwari Brajesh, Kottaisamy M. and Ramachandra Rao M. S.,"Structure, microstructure and physical properties of ZnO based materials in various forms: bulk, thin film and nano", J. Phys. D:Appl. Phys, Vol. 40, 6312, 2007.

Trivikrama Rao G. S., Tarakarama Rao D., "Gas sensitivity

of ZnO based thick film sensor to NH₃ at room temperature", Sens. Actuators B 55, 166-169,1999.

Xu J. Q., Pan Q. Y., Shun Y. A., Li Z., "Emulsion synthesis structure and gas sensing properties of nanometer ZnO", J. Inorg. Chem., Vol. 14: 355–359, 1998.

Yu J. H., Choi G. M., "Electrical and CO Gas Sensing Properties of ZnO-SnO₂ Composites", Sens. Actuatators B, 52, 251-256 ,1998.

Yuanhui Zheng , Chongqi Chen , Yingying Zhan , Xingyi Lin , Qi Zheng , Kemei Wei , Jiefang Zhu, and Yingjie Zhu, "Luminescence and Photocatalytic Activity of ZnO Nanocrystals: Correlation between Structure and Property", Inorganic Chemistry, Vol. 46 (16): 6675–6682 ,2007.

M. K. Deore (India, 1963) is an Associate Professor in Physics at Arts, Science and Commerce, College, Ozar(Mig), India. He received his M. Sc. degree in Physics in 1988 and Ph. D. degree in 2012 from the University of Pune, India. His topics of interest are gas sensors and nanomaterials.

G. H. Jain (India, 1965) is an Associate Professor in Physics and Head, Department of Physics. K. T . H. M. College, Nashik, India. He is the member of Board of Studies, University of Pune, India. He received his M.Sc. and Ph.D. degree in physics from the Uttar Maharashtra University, Jalgaon. His topics of interest are nanomaterial and gas sensor. Eight students are working for the Ph.D. degree on nonmaterial and gas sensor under his guidance.

Effects of Microwave Irradiation on Stability Characteristics of Water-Oil Emulsions

Adango Miadonye[*1], Emeka Nwankwor[2]

[*1]Department of Chemistry, Cape Breton University, Sydney, NS, Canada;
[2]Department of Process Engineering and Applied Science, Dalhousie University, Halifax, NS. Canada

[*1]adango_miadonye@cbu.ca; [2]e.nwankwor@dal.ca

Abstract

Petroleum is unquestionably the world's number one energy resource due to its wide end-use capabilities. However, the formation of water-oil emulsion is a problem of significant proportions in crude oil production that has decreased the overall oil recovery effeiciency and increased equipment corrosion, amongst others. In this project, we undertook an experimental study to determine the effects of microwave irradiation on the stability of water-in-oil emulsions from two Nigerian crude oil types and of varying water-oil volume ratios. The results showed that high water separation efficiency is attainable by this demulsification approach in all the four water-oil emulsions. It is also shown that better demulsification results are generally achieved with water-oil emulsions of higher water-phase volume ratio when the emulsions are subjected to equal irradiation exposure time and power.

Introduction

The production of oil from petroleum reservoirs involves all the processes that are aimed at depleting or draining the reservoir. Usually, the recovery of oil during production is broadly divided into primary, secondary and tertiary recovery processes. During the production and processing of crude oil, the formation of stable water-oil emulsion is completely undesirable. An emulsion is a heterogeneous aqueous system, containing at least one immiscible liquid intimately dispersed in another liquid in the form of droplets of diameter in the range of 0.1–20 microns, and stabilized by an emulsifying agent. For the specific case of water-oil emulsion, the stabilizing agents include asphaltenes, resins and wax. The dispersed droplets are known as the internal phase, while the liquid surrounding the dispersed droplets is referred to as the external or continuous phase. According to Kenneth (1998), the emulsifying agent separates the dispersed droplets from the continuous phase. The emulsion resulting from the production of oil often consists of crude oil as dispersion medium and water as dispersed phase, normally stabilized by heavy carbon components of the crude oil (which acts as a facilitator) such as asphaltenes, resins, and waxes (Sjoblom et al. 1990; Schramm, 1992). The stability of water-oil emulsion is arguably hinged on the relative difficulty associated with separating one of the phases from the other when the fluid is under some form of external stimuli; therefore, the stability of water-oil emulsions is a very complex problem.

Many industrial processes of demulsification have been employed in one application or the other including chemical and electromagnetic processes (Chen and He, 2003; Rajakovic and Skala, 2006; Selvarajan et al., 2001; and Eow et al., 2001). The first application of microwave irradiation as an emulsion separation technique was by the pioneering works of Klaila (1978) and Wolf (1986). Since then, there has been a significant number of research interests in this technique (Fang and Lai (1995); Fortuny et al. (2007); Anisa and Nour (2009); Huda and Nour (2011); Abdulbari et al. (2011); and Nour et al. (2012)). The effects of inorganic salts and inorganic acids in microwave demulsification of water-oil emulsions were investigated by Chan and Chen (2002). According to the authors, the separation efficiency as well as the demulsification rate are enhanced with increasing concentration of inorganic acids and also

with the inorganic salt (NaCl, KCl, NaNO₃, and Na₂SO₄) concentration in dilute range (<0.5 M). Using water-n-decane emulsion, Xia et al. (2004) studied the role of asphaltenes and resins on the stability of emulsion during microwave demulsification process. In their study on the dielectric and volumetric heating properties of microwave irradiation with respect to varying phase volume ratio and radiation time, Anisa and Nour (2009) showed that the rate of temperature increase decreases the dielectric properties and volumetric heat generated. The findings from Abdulbari et al. (2011) showed that emulsion stability was related to surfactant concentration, stirring time, temperature, the water-to-oil phase ratio and agitation speed. Nour et al. (2012), performed comparative analyses of the demulsification of water-oil emulsion using microwave irradiation energy and conventional thermal heating by comparing the percentage of water separated, and droplets size distribution in each crude oil.

In this project, we investigated the effects of microwave irradiation on the stability characteristics of water-oil emulsion of two Nigerian crude oils, thus, determined the water separation efficiency attainable by deploying this method of water-oil emulsion demulsification.

Experimental

The emulsions were prepared from two crude oil samples - *Antan Blend* and *Qua Iboe;* the physical properties of these crude samples are given in Tables 1:

TABLE 1: PHYSICAL PROPERTIES OF THE CRUDE OIL SAMPLES

Properties	Antan Blend	Qua Iboe
API gravity	20.6	35.2
Specific gravity	0.9306	0.8487
Sulphur content (%)	0.36	0.13
Viscosity @40°C (cSt.)	11.05	3.92
Neut. number (TAN)	0.48	0.32
Wax content (%)	4.87	-
Asphaltene content (%)	0.24	-
Salt content (%)	4.6	10.8

To prepare the 50-50% water-oil emulsion, 200ml of crude oil was poured into 900ml graduated beakers made of thermal-stable borosilicate glass, and 20ml of the surfactant, sodium dodecyl sulphate (SDS) purchased from Sigma-Aldrich, Canada, was added into the crude oil in the beaker. With the aid of a three-blade 750 rpm rated propeller, the oil and surfactant

mixture was vigorously agitated at laboratory temperature (29°C) for a duration of 120 seconds. Then 200ml of clean tap water was slowly added into the beaker and the mixture was agitated for ten minutes with the propeller to facilitate homogenization. Subsequently, a droplet of the resulting emulsions placed on a filter paper did not disperse which confirmed the formation of water-oil emulsion.

The emulsion was allowed to settle for a period of 2.5 hours, the volume of sedimented water was read and recorded repeatedly every 15 minutes interval. The emulsion was further agitated for 5 minutes before been irradiated in a domestic microwave oven Dandy model DMW 1048SS for 150 seconds. The rated power output of the microwave oven is 1000W, and its operating voltage and frequency are 4.15KV and 2450MHz respectively.

Results and Discussion

Antan Blend Emulsion (ABE)

The results from water sedimentation in the three 100ml measuring cylinders before and after the microwave irradiation demulsification process are given in Figure 1 for the 50-50% water-oil emulsion, as a typical example. The relative volume of sedimented water for any of these emulsions (both before and after microwave irradiation) is a practical indicator of the stability of the emulsion. This is because the stability (or otherwise) of an emulsion is the ability of the emulsion to separate into its constituting continuous (oil) and dispersed (water) phases. In the 50-50% water-oil emulsion the average volume of water sedimentation was 14.6ml after a period of 2.5 hours. However, when the same emulsion sample was exposed to microwave irradiation for 150 seconds, an average volume of 44.7ml of water was recorded at the bottom of the measuring cylinder. This is over 200% of water sedimentation after microwave irradiation.

For the 30-70% water-oil emulsion, the average volume of water settled at the bottom of the measuring cylinder after 2.5 hours of sedimentation was 7.67ml, and after a 150-second microwave demulsification process only 33% increment in water sedimentation was obtained.

The water separation efficiency (WSE) of the emulsion before and after the microwave irradiation demulsification process is computed as follows:

$$WSE = \frac{\text{average volume of settled water}}{\text{pro-rated volume of original water volume}} \times 100\%$$

Figure 2 compared the values obtained before and after both emulsion types were subjected to microwave demulsification process.

It can be seen from Figure 2 that the 30-70% water-oil emulsion attained a maximum water separation efficiency of 77.8% which is below the 89.4% separation efficiency attained by the 50-50% water-oil emulsion. Since water separation efficiency is inversely proportional to stability, it therefore follows that the 30-70% water-oil emulsion is more stable than the 50-50% water-oil emulsion. This is in agreement with Figure 2 – the more stable emulsions are at the lower part, while the unstable 50-50% water-oil *ABE* is at the uppermost part of the graph.
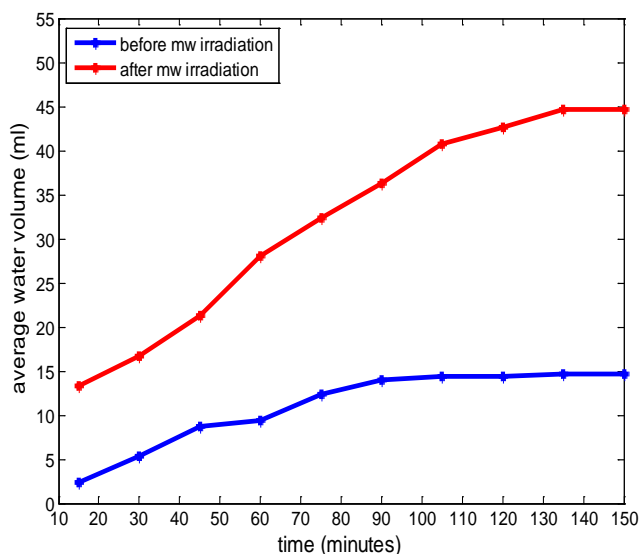

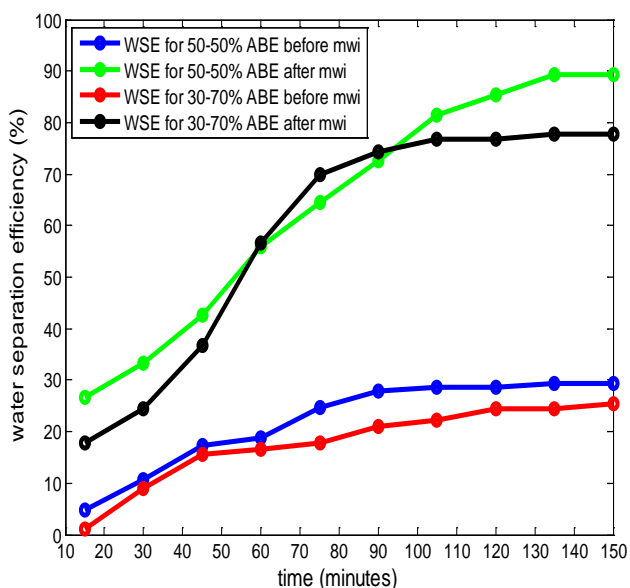FIG. 1AVERAGE WATER VOLUME SEDIMENTED BEFORE AND AFTER MICROWAVE IRRADIATION WITH TIME FOR 50-50% ABE

FIG. 2 COMPARISON OF WATER SEPARATION EFFICIENCY FOR ABE

Qua Iboe Emulsion (QIE)

The results obtained for 50-50% and 30-70% water-oil emulsions prepared from *Qua Iboe* crude oil were similar to those of *ABE*. Figures 3 and 4 depicted the volume of sedimented water and water separation efficiency, respectively; attained both before and after the emulsions were subjected to microwave demuls-ification process.
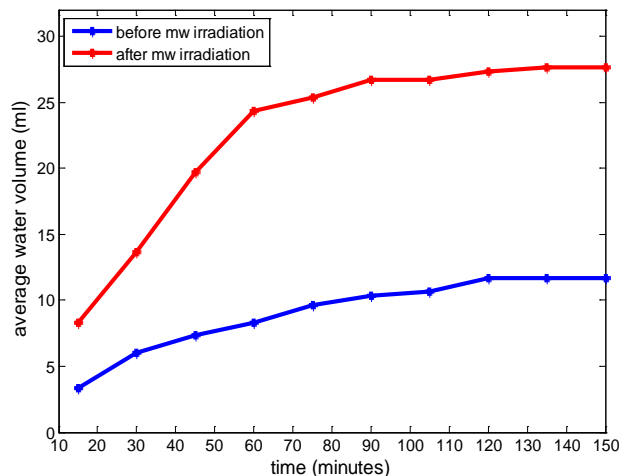

FIG. 3 AVERAGE WATER VOLUME SEDIMENTED BEFORE AND AFTER MICROWAVE IRRADIATION WITH TIME FOR 30-70% QIE
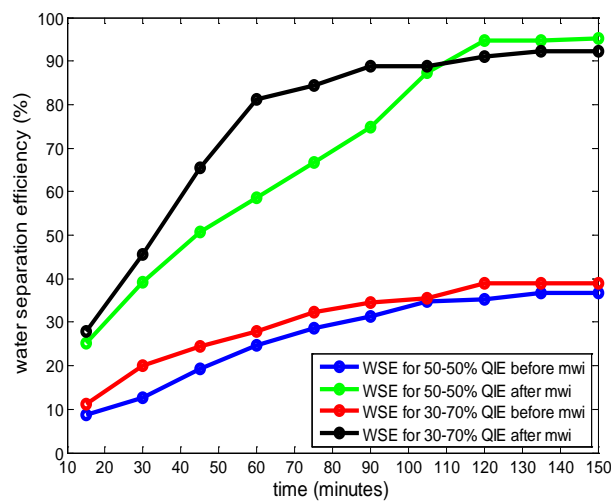

FIG. 4 COMPARISON OF WATER SEPARATION EFFICIENCY FOR QIE

In the 50-50% water-oil emulsion, an average volume of 18.33ml of water was obtained after a sedimentation period of 2.5 hours. After the emulsion was exposed to microwave irradiation for 150 seconds, the average volume of water obtained (after same time interval of 2.5 hours) rose to 47.67ml. For the 30-70% water-oil emulsion (Figure 3), the average volume of water obtained after 2.5 hours of sedimentation was 11.67ml before irradiation and 26.67ml after irradiation. This is approximately 44% and significantly lower than the

160% increment obtained in 50-50% *QIE*.

The water separation efficiency for the 50-50% and the 30-70% *QIE* were 95.3% and 92.2% respectively (Figure 4). It is evident from the results that the 30-70% *Qua Iboe* crude oil emulsion is slightly more stable than the 50-50% *QIE,* since water separation efficiency has an inverse correlation with emulsion stability.

Comparison of Stability of the Emulsions

The water separation efficiency for the 50-50% water-oil emulsions formed from *Anten Blend* and *Qua Iboe* crude oil are compared to those for 30-70% emulsion. Figures 5 and 6 illustrate the plots of the water separation efficiency against time (before and after microwave irradiation) for emulsions of the same water and oil ratio. On the evidence of both graphs, it is clear to see that irrespective of water-oil ratio, the emulsions prepared from *Antan Blend* crude oil are generally more stable than emulsions prepared from *Qua Iboe* crude oil sample.
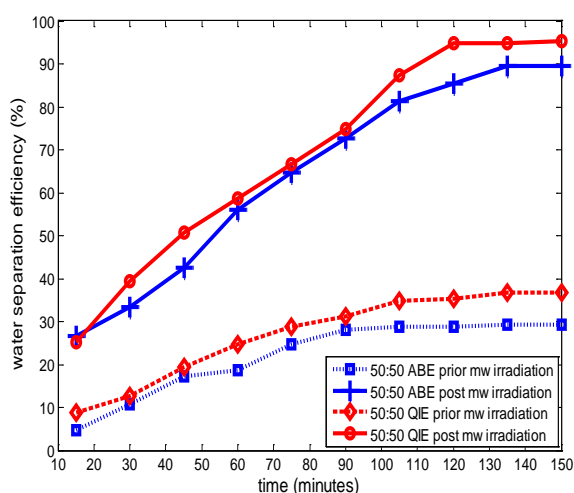

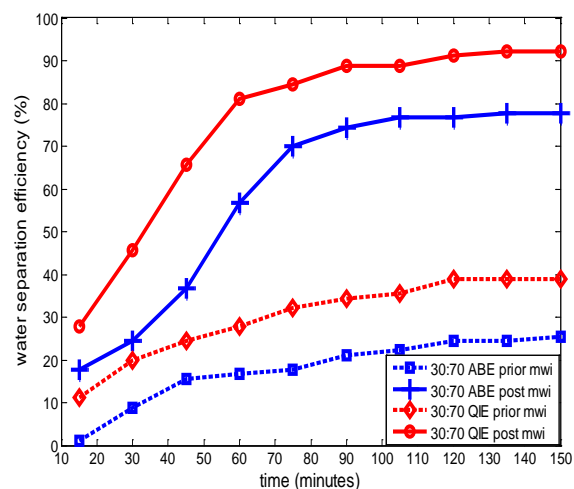FIG. 5 COMPARISON OF WATER SEPARATION EFFICIENCY FOR 50-50% OIL EMULSIONS

FIG. 6 COMPARISON OF WATER SEPARATION EFFICIENCY FOR 30-70% OIL EMULSIONS

According to Stoke's law, the magnitude of the settling velocity of water droplets (dispersed phase) in a continuous phase such as oil is proportional to the the squared diameter of the water droplets, difference between the densities of the dispersed phase and continuous phase (a direct function of the specific gravities of both phases, and inversely proportional to the dynamic viscosity of the continuous phase. It, therefore means that the stability of water-oil emulsions is reduced by any mechanism that results either in increasing of the density difference between the phases and/or reduction in the dynamic viscosity of the continuous phase. From Table 1, it is evident that the density difference between the dispersed phase and the *Qua Iboe* crude is higher than the density difference between the dispersed phase and the *Antan Blend* crude. Also, the viscosity of the *Qua Iboe* crude is lower than that of the *Antan Blend* crude sample. These are in agreement with Figures 5 and 6 which depicted that the water-oil emulsions from *Antan Blend* crude are more stable than those from *Qua Iboe* crude sample of equal water-oil proportions.

The presence of microwave irradiation significantly increased the water separation efficiency of the emulsion, thus reduced the stability of the water-oil emulsions. This is due to the quadratic dependence of the settling velocity on the droplet diameter thus, any process or mechanism that increases the size of the droplet diameter would invariably lead to significant increase in phase separation and reduction in emulsion stability. The fast and volumetric heating effects provided by the use of microwave irradiation ultimately results to droplet diameter growth and lower fluid viscosity which facilitate a rapid emulsion separation process.

Conclusions

The results of the experiments conducted for the four different water-oil emulsions indicate that microwave irradiation is undoubtedly an effective means for emulsion demulsification. The water separation efficiency of all emulsions increased with increasing separation time; and importantly, the separation time for all the four water-oil emulsions used was significantly enhanced upon exposing the emulsions to microwave irradiation. The *Antan Blend* crude oil sample which has higher viscosity and contains asphaltenes resulted in the emulsions that are more stable than the *Qua Iboe* crude oil emulsions. Furthermore, the 30-70% emulsions were generally more stable than the 50-50% emulsions from the same

crude oil samples. As evident in the high water separation efficiency attained, microwave irradiation process offers a unique and characteristic cheap, clean, fast and volumetric heating effect that accelerates water-oil emulsion separation by reducing viscosity and enhancing gravity sedimentation.

ACKNOWLEDGMENT

REFERENCES

Abdulbari, H.A., Abdurahman, N.H., Rosli1, Y.M., Mahmood, W.K., Azhari, H.N. Demulsification of petroleum emulsions using microwave separation method, International Journal of the Physical Sciences Vol. 6(23), (2011) 5376-5382.

Anisa, A.N.I., Nour, A.H. "Emulsion Separation Rate Enhancement via Microwave Heating Tech"., National Conference on Postgraduate Research (NCON-PGR), UMP Conference Hall, Malaysia. 2009.

Chan, C. C., Chen, Y. C. Demulsification of W/O emulsions by microwave radiation. Sep. Sci. Technol. 37 (15), (2002) 3407-3420.

Chen, G., He, G. Separation of water and oil from water-in-oil emulsion by freeze/thaw method. Sep. Purif. Technol. 31, (2003) 83-89.

Eow, J. S., Ghadiri, M., Sharif, A. O., Williams, T. J. Electrostatic enhancement of coalescence of water droplets in oil: a review of the current understanding. Chemical Engineering Journal 84 (3), (2001) 173–192.

Fang, C. S., Lai, P. M. C. Microwave heating and separation of water-in-oil emulsion. J. Microw. Power Electromagn. Energy, 30 (1), (1995) 46-57.

Fortuny, M., Oliveira, C. B. Z., Melo, R. L. F. V., Nele, M., Coutinho, R. C. C., Santo, A. F. Effect of salinity, temperature, water content, and pH on the microwave demulsification of crude oil emulsion. Energy & Fuels 21, (2007) 1358-1364.

Huda, S.N., Nour, A.H. Microwave Separation of Water-In-Crude Oil Emulsions, International Journal of Chemical and Environmental Engineering, 2,(1), (2011) Page 36-41.

Kenneth J. Lissant, "Emulsification and De-emulsification, A Historical Overview", Colloids and surfaces, 29, (1998)

Klaila, W. J. Method and apparatus for controlling fluency of high viscosity hydrocarbon fluids. US Patent 4,067,683, January 10, 1978.

Nour, A.H., Anisa, A.N.I., Nour, A.H. Demulsification of water-in-oil (W/O) emulsion via microwave irradiation: An optimization, Scientific Research and Essays Vol. 7(2), (2012) 231-243.

Rajakovic, V., Skala, D. Separation of water-in-oil emulsions by freeze/thaw method and microwave radiation. Sep. Purif. Technol. 49, (2006) 192-196.

Schramm, L. L. Petroleum Emulsion. In.: Schramm, L.L. Emulsions Fundamentals and Applications in the Petroleum Industry, 1-45. American Chemical Society, Washington DC. 1992.

Selvarajan R., Anantha subramaniam S., and Robert A. M. "Aqueous Dispersion of an Oil Soluble Demulsifier for Breaking Crude Oil Emulsions", (US Patent No. 6,294,093), (2001).`

Sjoblom, J., Ming Yuan, L., Hoiland, H and Johansen, J.E. Water-in-Crude Oil Emulsions from the Norwegian Continental Shelf, Part III. A Comparative Destabilization of Model Systems. Surfaces. 46, (1990) 127-139.

Wolf, N. O. Use of microwave radiation in separating emulsion and dispersion of hydrocarbons and water. US Patent 4,582,629, April 15, 1986.

Xia, L. X., Lu, S. W., Cao, G. Y., 2004. Salt-assisted microwave demulsification. Chem. Eng. Commun. 191, 1053-1063.

Adango Miadonye is a Professor of Chemical Engineering and the Chair of Department of Chemistry at Cape Breton University. He joined Cape Breton University in 1998 after many years of university teaching and research experience in Chemistry, Chemical Engineering and Petroleum Engineering in several countries. He is a member of editorial boards of several journals for chemical engineering , and petroleum science and engineering, and served as Chair in several Research Award Selection Committees for Government and Private sectors. Dr. Miadonye is an adjunct Professor at the Department of Process Engineering and Applied Science, Dalhousie University.

Numerical Study of the Impact of Complex Fracture Patterns on Well Performance in Shale Gas Reservoirs

Wei Yu[*1], Bo Gao[2], Kamy Sepehrnoori[1]

[1]Department of Petroleum and Geosystems Engineering, The University of Texas at Austin, TX 78712, USA
[2]ExxonMobil Upstream Research Company, Houston, Texas, USA

[*1]yuwei127@gmail.com; [2]b.robert.gao@gmail.com; [3]kamys@mail.utexas.edu

Abstract

There is generally a high uncertainty in identifying fracture patterns due to fracture interference in shale gas reservoirs. In this work, we studied five complex and irregular hydraulic fracture patterns within one perforation stage, where the fracture half-length varies, and compared well performance using a commercial reservoir simulator. Results show that there is a big difference in gas recovery between different patterns. We also studied the effects of matrix permeability, cluster spacing and fracture conductivity on reservoir performance. This work will provide critical insights into characterization of hydraulic fracture geometry in shale gas reservoirs.

Keywords

Barnett Shale; Fracture Pattern; Sensitivity Study; Gas Desorption; Geomechanics

Introduction

Horizontal drilling and hydraulic fracturing are two key enabling technologies for economic gas production in shale reservoirs. A large contact area between fractures and reservoir created by hydraulic fracturing plays a major role in economic shale gas production. Despite the recent success in shale gas development, the cost of hydraulic fracturing treatment remains very high. Therefore, optimization of hydraulic fracture treatment design is clearly desirable. There have been many attempts in recent years to optimize fracturing treatment design for shale gas reservoirs (Wilson and Durlofsky, 2012; Meyer et al., 2013; Wang et al., 2013; Yu and Sepehrnoori, 2013a). In most of the reviewed works, the optimum design is based on the assumption of equal fracture half-length. However, the fracture geometry is

uncertain and very challenging to be measured exactly, even with microseismic technique and chemical tracer approach. Also, many recent attempts have been made to model multiple hydraulic fractures propagation and predict fracture geometry (Wu et al., 2012; Olson and Wu, 2012; Xu and Wong, 2013; Wu and Olson, 2013a, 2013b). However, the validation with real fracture geometry for these models is very challenging. Hence, there is a very high uncertainty in fracture pattern characterization. Hence, optimization of fracturing design with large uncertainties in fracture patterns for shale reservoirs remains a challenge.

In this work, we proposed five different hydraulic fracture patterns within one perforation stage and use CMG-IMEX (2012) to simulate and compare the well performance of these patterns. We verified our numerical simulation method using field data from Barnett Shale by considering gas desorption and geomechanics effects. The effects of matrix permeability, cluster spacing, and fracture conductivity are investigated. The goal of this work is to evaluate the impact of uncertainty in fracture pattern on well performance and provide critical insights into characterization of hydraulic fracture geometry in shale gas reservoirs.

Reservoir Modeling including Hydraulic Fractures

Reservoir simulation is the preferred approach to evaluate well performance of shale gas reservoirs. CMG-IMEX (2012) is used to model hydraulic fractures and gas flow in a shale gas reservoir. In our

simulation study, there is no water flow and only gas is flowing into the wellbore through the hydraulic fractures by considering non-Darcy effect. The non-Darcy Beta factor, used in the Forchheimer number, is determined using a correlation proposed by Evans and Civan (1994). Local grid refinement (LGR) with logarithmic cell spacing is used in the simulation to accurately model flow from the shale to the fracture. This method can accurately model transient gas production from hydraulic fractures in shale gas reservoirs (Rubin, 2010; Cipolla et al., 2010; Yu and Sepehrnoori, 2013b, 2014; Yu et al., 2014).

Model Validation Using Barnett Field Data

Once a numerical hydraulic fracture model has been developed, it should be validated to ensure high reliability of simulation results. In this work, a field production dataset from Barnett Shale was used to perform history matching in order to validate hydraulic fracture model (Grieser, et al., 2009). The accurate static and dynamic rock properties required by reservoir simulation model can be derived from core samples (Xu and Torres-Verdin, 2013) or well logs (Xu et al., 2013). Detailed reservoir information about the Barnett Shale well is listed in Table 1.

TABLE 1 BARNETT SHALE RESERVOIR INFORMATION

Parameter	Value(s)	Unit
The model dimensions (L×W×H)	3000×1500×300	ft
Initial reservoir pressure	3800	psi
Bottom hole pressure	1500	psi
Production time	5	year
Reservoir temperature	180	ºF
Gas viscosity	0.02	cP
Reservoir depth	7000	ft
Pore pressure gradient	0.54	psi/ft
Closure pressure	5000	psi
Closure pressure gradient	0.71	psi/ft
Matrix permeability	0.00001	md
Matrix porosity	0.04	value
Initial gas saturation	0.70	value
Compressibility of shale	10^{-6}	psi^{-1}
Fracture spacing	100	ft
Fracture conductivity	1	md-ft
Fracture half-length	245-595	ft
Fracture height	300	ft
Horizontal well length	2120	ft
Langmuir volume	96	scf/ton
Langmuir pressure	650	psi
Bulk density	2.58	g/cm3

Gas desorption is described by the Langmuir isotherm with Langmuir pressure of 650 psi and Langmuir volume of 96 scf/ton (Mengal and Wattenbarger, 2011). Geomechanics of hydraulic fractures, i.e. stress-

dependent fracture conductivity, is also considered using a specific compaction table, accounting for the decreasing conductivities of propped fractures with an increase in closure stress or decrease in pressure, as shown in Fig. 1. In this well, the fracture half-length is varying: predictions of various values of fracture half-length were provided by the fracture maps obtained by using geophones installed in offset wells (Grieser, et al., 2009; Yu and Sepehrnoori, 2013c). Reservoir modeling including hydraulic fractures for this well is shown in Fig. 2. Fig. 3 presents the history matching results with and without considering gas desorption and geomechanics effects. It can be seen that a reasonable match between the numerical simulation results and the actual field data is obtained for all cases. The difference between each case is small.
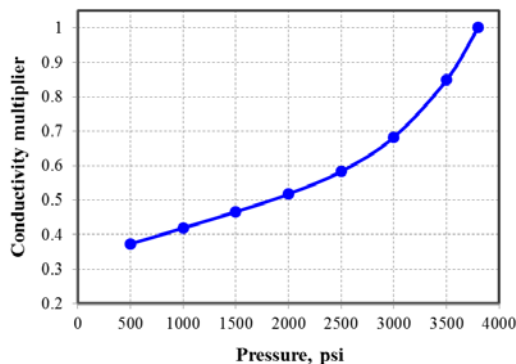

FIG. 1 FRACTURE CONDUCTIVITY MULTIPLIER VERSUS PRESSURE FOR BARNETT SHALE
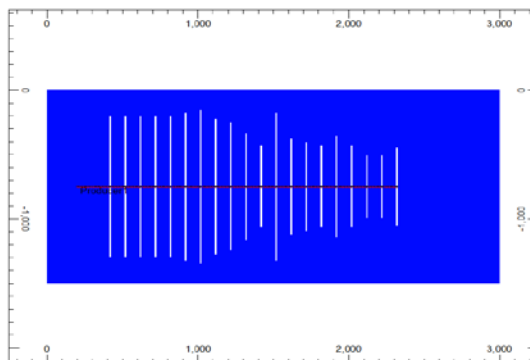

FIG. 2 A BARNETT SHALE WELL WITH VARYING HYDRAULIC FRACTURE HALF-LENGTH
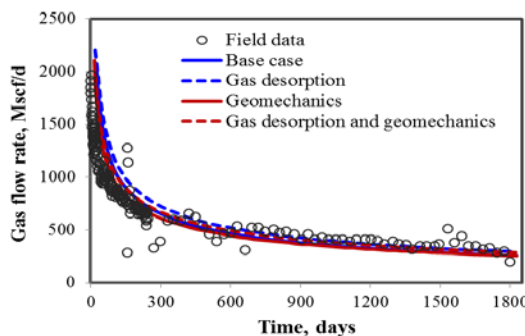

FIG. 3 HISTORY MATCHING RESULTS

After history matching, we performed production forecasting for a 30-year period. As shown in Fig. 4, the gas desorption contributes to 11% of total gas production after 5 years of field production, and 20% of total gas production at 30 years of gas production. However, geomechanics lowers the production by 6% of total gas production after 5 years, and 2% of total gas production after 30 years. Finally, the effect of combining gas desorption and geomechanics contributes to 3.4% increase in total gas production after 5 years and 16.6% increase in total gas production after 30 years. Henceforth, gas desorption had a positive effect and geomechanics had a negative impact on gas production in this case study. Fig. 5 shows the pressure distribution at end of field production, clearly illustrating the drainage area between hydraulic fractures and reservoir in this horizontal fractured Barnett Shale well.
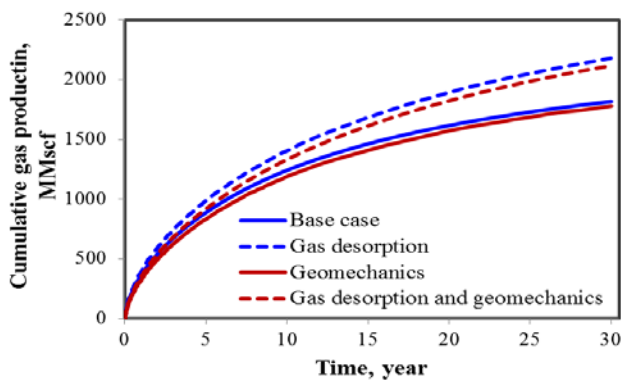

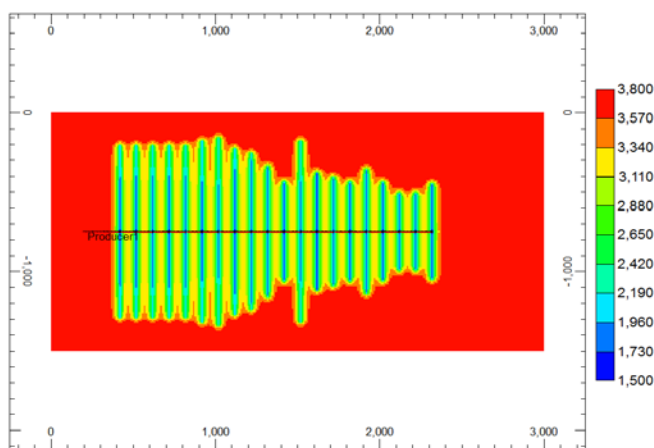FIG. 4 PRODUCTION FORECASTING RESULTS

FIG. 5 PRESSURE DISTRIBUTION AT END OF FIELD PRODUCTION

Impact of Fracture Pattern on Well Performance

In this work, we presented five complex hydraulic fracture patterns with varying fracture half-length within one perforation stage, as illustrated in Fig. 6.

Five clusters within one perforation stage are assumed. The total fracture length remains the same for each fracture pattern (5000 ft). The details for individual fracture half-length in each case are described below.

Case 1: Five fractures with an equal half-length of 500 ft.

Case 2: Middle fracture with a half-length of 740 ft, two longer fractures with a half-length of 500 ft, and two shorter fractures with a half-length of 380 ft.

Case 3: Two longer fractures with a half-length of 740 ft, and three shorter fractures with a half-length of 340 ft.

Case 4: Middle fracture with a half-length of 220 ft, two shorter fractures with a half-length of 400 ft, and two longer fractures with a half-length of 740 ft.

Case 5: Three longer fractures with a half-length of 740 ft, and two shorter fractures with a half-length of 140 ft.
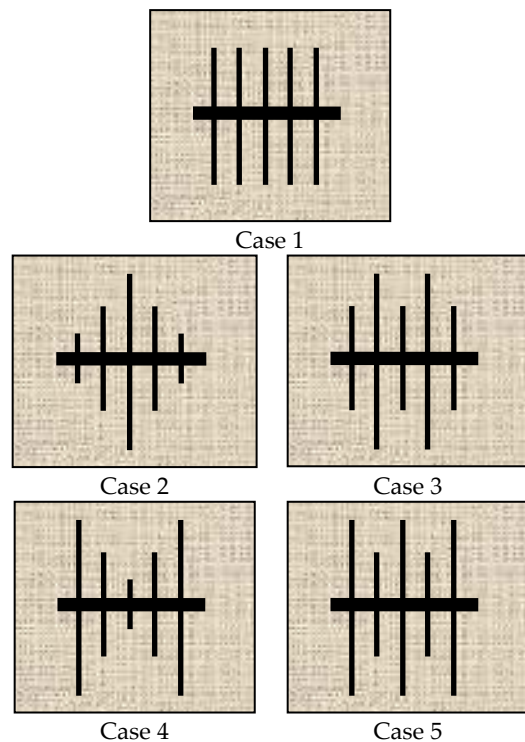
FIG. 6 FIVE DIFFERENT HYDRAULIC FRACTURE PATTERNS WITHIN ONE PERFORATION STAGE UNDER THE SAME TOTAL FRACTURE LENGTH OF 5000 FT

We set up another shale gas reservoir model with a volume of 2000 ft × 2000 ft × 300 ft based on average reservoir data from Barnett Shale, as listed in Table 2. Cluster spacing for each case is set at 80 ft. Gas desorption effect and stress-dependent fracture conductivity illustrated in Fig. 1 are considered in all

subsequent simulations.

TABLE 2 PARAMETERS USED IN SIMULATIONS FOR BARNETT SHALE

Parameter	Value(s)	Unit
The model dimensions (L×W×H)	2000×2000×300	ft
Initial reservoir pressure	3800	psi
Bottom hole pressure	1000	psi
Production time	30	year
Reservoir temperature	180	ºF
Gas viscosity	0.02	cP
Matrix permeability	0.0001	md
Matrix porosity	0.06	value
Initial gas saturation	0.70	value
Compressibility of shale	10^{-6}	psi^{-1}
Cluster spacing	80	ft
Stage spacing	400	ft
Fracture conductivity	100	md-ft
Fracture height	300	ft
Langmuir volume	96	scf/ton
Langmuir pressure	650	psi
Bulk density	2.58	g/cm3

Comparisons of gas flow rate and gas recovery at 30 years of production between these five cases are presented in Figs. 7 and 8, respectively.
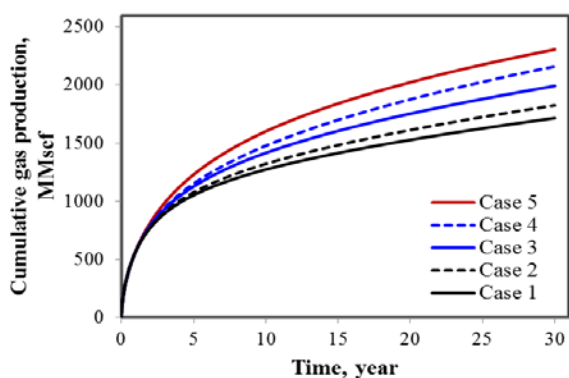

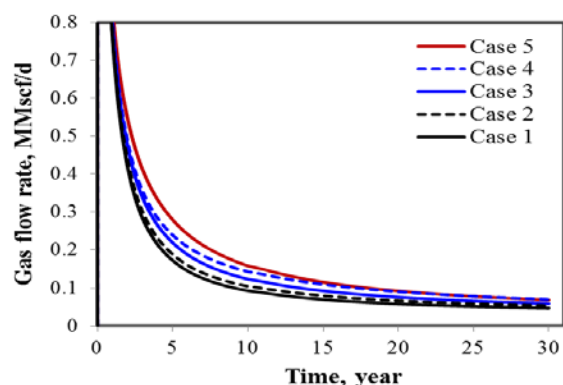FIG. 7 COMPARISON OF CUMULATIVE GAS PRODUCTION WITH FIVE CASES

FIG. 8 COMPARISON OF GAS FLOW RATE WITH FIVE CASES

As shown in Figs. 7 and 8, at early production time (less than 2 years), the well performance for each case remains the same, since the same total fracture length leads to the same contact area between fractures and

reservoir before fracture interference occurs. However, after 2 years of production, the well performance for each case is very different. Among the five cases, Cases 1 and 5 show the lowest and the highest gas flow rate and gas recovery, respectively. The absolute and relative difference of gas recovery at 30 years of production between Cases 1 and 5 are around 591 MMscf and 35%, respectively. The gas recovery in Case 3 is larger than that of Case 2 and Case 4 performs better than Case 3. This is simply because Cases 1 and 5 have the strongest and the weakest fracture interference, respectively. This may suggest that when performing history matching with short-term period of gas production, a good agreement can be obtained with each fracture pattern; while there will be a big uncertainty at late time of production because of the different degree of fracture interference. Therefore, it may imply that the hydraulic fracture pattern can be characterized based on history matching with long-term period of gas production.
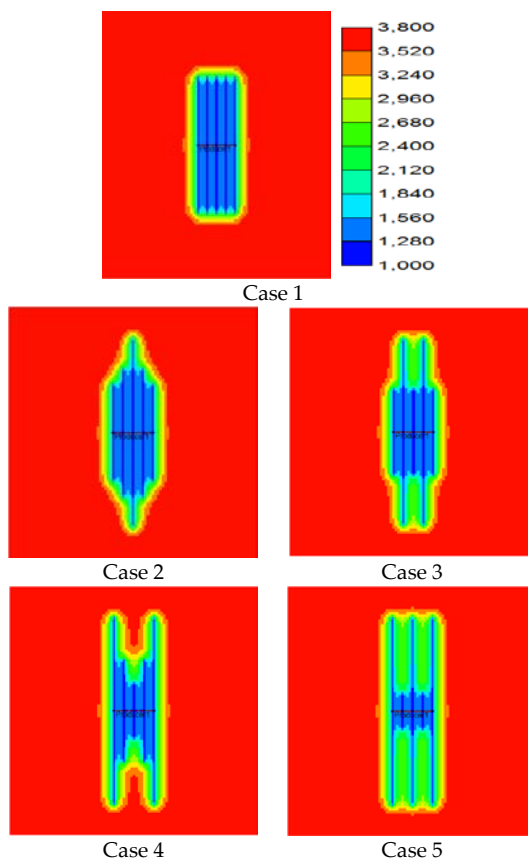

FIG. 9 PRESSURE DISTRIBUTION OF FIVE CASES AT 4 YEARS OF GAS PRODUCTION (CLUSTER SPACING OF 80 FT)

Fig. 9 shows pressure distribution of these five cases after four years of production. Clearly, Case 1 has the smallest drainage area between fractures and reservoir, leading to the lowest gas recovery, and Case 5 shows the largest drainage area, leading to the

highest gas recovery. The drainage area in Cases 2, 3, and 4 with the same total fracture length are between Cases 1 and 5. The drainage area in Case 4 is larger than that in Cases 2 and 3. It suggests that longer outer fractures lead to larger drainage area and higher gas recovery from low permeability shale gas reservoirs.

Sensitivity Study

Effect of Matrix Permeability

The shale matrix permeability plays an important role in gas recovery in a hydraulic fractured horizontal well. The matrix permeability values of 50 nD and 500 nD are investigated with cluster spacing of 80 ft and fracture conductivity of 100 md-ft. Figs. 10 and 11 show the comparison of gas recovery for matrix permeability of 50 nD and 500 nD, respectively. As shown, the transition time of well performance change corresponding to permeability of 50 nD and 500 nD is around 3 years and 0.5 year, respectively, and the absolute difference of gas recovery at 30 years of production is about 434 MMscf and 866 MMscf, respectively. Hence, the gas recovery increases with the increasing shale matrix permeability. It means that proper characterization of hydraulic fracture pattern is very significant in shale reservoirs with higher matrix permeability.
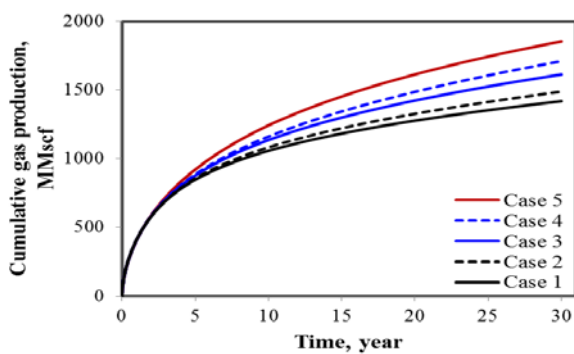
FIG. 10 COMPARISON OF CUMULATIVE GAS PRODUCTION WITH PERMEABILITY OF 50 ND
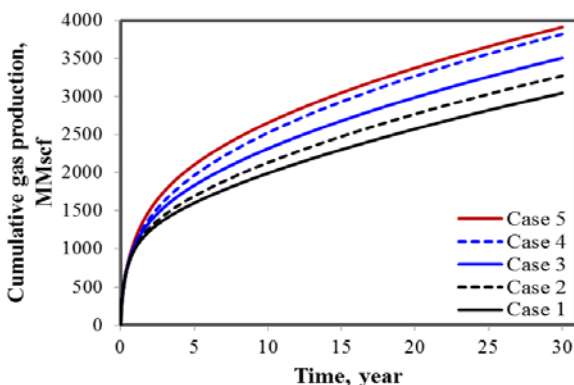
FIG. 11 COMPARISON OF CUMULATIVE GAS PRODUCTION WITH PERMEABILITY OF 500 ND

Effect of Cluster Spacing

Cluster spacing in each stage of a hydraulic fracturing stimulation treatment is very important. The cluster spacing values of 60 ft and 100 ft are investigated with matrix permeability of 100 nD and fracture conductivity of 100 md-ft. The comparison of gas recovery for cluster spacing of 60 ft and 100 ft is shown in Figs. 12 and 13, respectively. It can be seen that the transition time of well performance change corresponding to cluster spacing of 60 ft and 100 ft is around 1 year and 2.5 years, respectively, and the absolute difference of gas recovery at 30 years of production is about 550 MMscf and 600 MMscf, respectively. For all cases, the gas recovery increases slightly with the increasing cluster spacing.
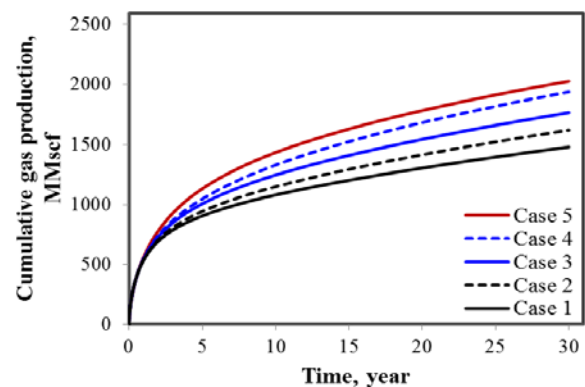
FIG. 12 COMPARISON OF CUMULATIVE GAS PRODUCTION WITH CLUSTER SPACING OF 60 FT
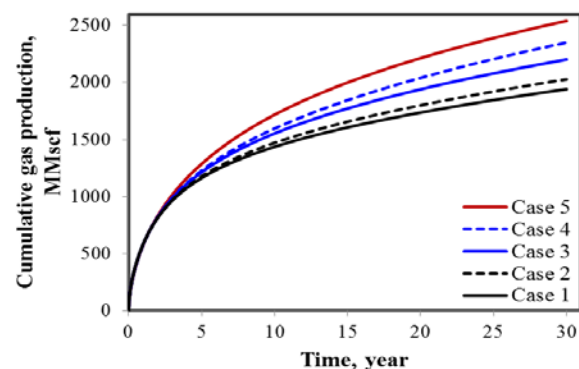
FIG. 13 COMPARISON OF CUMULATIVE GAS PRODUCTION WITH CLUSTER SPACING OF 100 FT

Effect of Fracture Conductivity

Fracture conductivity is defined as fracture width multiplied by fracture permeability. The fracture conductivity values of 1 md-ft and 10 md-ft are investigated with cluster spacing of 80 ft and matrix permeability of 100 nD. Figs. 14 and 15 show the comparison of gas recovery for fracture conductivity of 1 md-ft and 10 md-ft, respectively. As shown, the transition time of well performance change

corresponding to fracture conductivity of 1 md-ft and 10 md-ft is around 13 years and 3 years, respectively, and the absolute difference of gas recovery at 30 years of production is about 140 MMscf and 500 MMscf, respectively. Hence, the gas recovery is very sensitive to the fracture conductivity, increasing significantly with the increasing fracture conductivity. It implies that quantification of fracture conductivity is very critical in characterization hydraulic fracture pattern.

FIG. 14 COMPARISON OF CUMULATIVE GAS PRODUCTION WITH FRACTURE CONDUCTIVITY OF 1 MD-FT

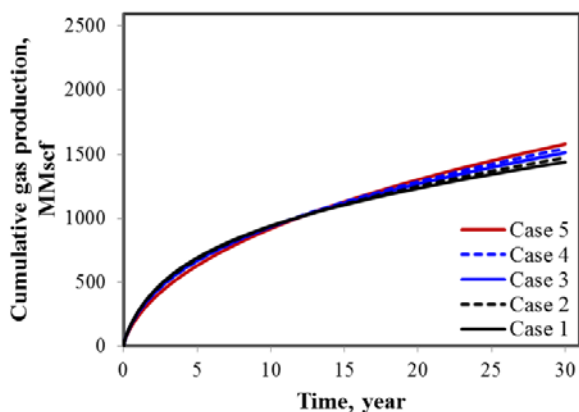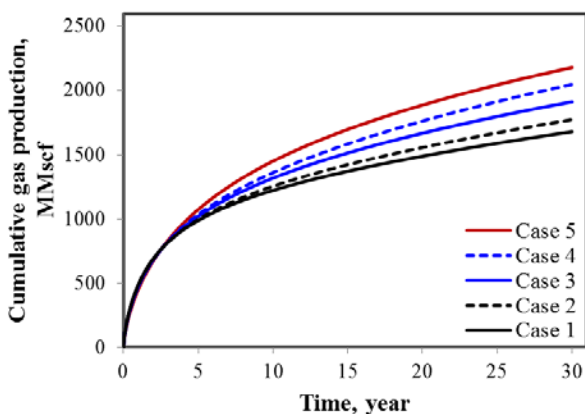FIG. 15 COMPARISON OF CUMULATIVE GAS PRODUCTION WITH FRACTURE CONDUCTIVITY OF 10 MD-FT

Conclusions

We proposed five different and likely fracture patterns within one perforation stage in a shale gas well and performed a series of simulations studying considering gas recovery. The simulation results show that there exists a big difference between these five fracture patterns in terms of recovery; the difference increases significantly with increasing matrix permeability, fracture conductivity, and to a lesser extend with increasing cluster spacing. The characterization of hydraulic fracture pattern is very important in shale reservoirs with higher permeability and larger fracture conductivity.

REFERENCES

Cipolla, C.L., Lolon, E.P., Erdle, J.C., and Rubin, B. "Reservoir Modeling in Shale-Gas Reservoirs." SPE Reservoir Evaluation & Enginerring 13 (2010): 638–653.

CMG: "IMEX User's Guide." Computer Modeling Group Ltd, 2012.

Evans, R.D., and Civan, F. "Characterization of Non-Darcy Multiphase Flow in Petroleum Bearing Formations." Report, U.S. DOE Contract No. DE-AC22-90BC14659, School of Petroleum and Geological Engineering, University of Oklahoma, 1994.

Grieser, B., Shelley, B., and Soliman, M. "Prediction Production Outcome from Multi-stage, Horizontal Barnett Completions." Paper SPE 120271 presented at SPE Production and Operations Symposium, Oklahoma, OK, April 4–8, 2009.

Mengal S.A., and Wattenbarger, R.A. "Accounting for Adsorbed Gas in Shale Gas Reservoirs." Paper SPE 141085 presented at SPE Middle East Oil and Gas Show and Conference, Manama, Bahrain, September 25–28, 2011.

Meyer, B.R., Bazan, L.W., Brown, E.K., and Brinzer, B.C. "Key Parameters Affecting Successful Hydraulic Fracture Design and Optimized Production in Unconventional Wells." Paper SPE 165702 presented at SPE Eastern Regional Meeting, Pittsburgh, PA, August 20–22, 2013.

Olson, J.E., and Wu, K. "Sequential vs. Simultaneous Multizone Fracturing in Horizontal Wells: Insights from a Non-planar, Multifrac Numerical Model" Paper SPE 152602 presented at SPE Hydraulic Fracturing Technology Conference, The Woodlands, TX, February 6–8, 2012.

Rubin, B. "Accurate Simulation of Non-Darcy Flow in Stimulated Fractured Shale Reservoirs." Paper SPE 132093 presented at SPE Western Regional Meeting, Anaheim, CA, May 27–29, 2010.

Wang, F., Zhang, S., and Liu, B. "Pressure Transient Analysis of Multi-stage Hydraulically Fractured Horizontal Wells." Journal of Petroleum Science Research 2 (2013): 162–166.

Wilson, K.C., and Durlofsky, L.J. "Computational Optimization of Shale Resource Development Using Reduced-Physics Surrogate Models." Paper SPE 152946 presented at SPE Western Regional Meeting, Bakersfield, CA, March 19–23, 2012.

Wu, K. "Simultaneous Multi-frac Treatments: Fully Coupled Fluid Flow and Fracture Mechanics for Horizontal Wells." Paper SPE 167626 presented at SPE Annual Technical Conference and Exhibition, New Orleans, LA, September 30–October 2, 2013a.

Wu, K., and Olson, J.E. "Investigation of the Impact of Fracture Spacing and Fluid Properties for Interfering Simultaneously or Sequentially Generated Hydraulic Fractures." SPE Production & Operations 28 (2013b): 427–436.

Wu, R., Kresse. O., Weng, X., Cohen, C., and Gu, H. "Modeling of Interaction of Hydraulic Fractures in Complex Fracture Networks." Paper SPE 152052 presented at SPE Hydraulic Fracturing Technology Conference, The Woodlands, TX, February 6–8, 2012.

Xu, C., Heidari, Z., and Torres-Verdín, C. "Rock Classification in Carbonate Reservoirs Based on Static and Dynamic Petrophysical Properties Estimated from Conventional Well Logs." Paper SPE 159991 presented at SPE Annual Technical Conference and Exhibition, San Antonio, TX, October 5–9, 2012.

Xu, C., and Torres-Verdín, C. "Quantifying Fluid Distribution and Phase Connectivity with a Simple 3D Cubic Pore Network Model Constrained by NMR and MICP." Computers & Geosciences 61 (2013): 94–103.

Xu, G., and Wong, S.W. "Interaction of Multiple Non-planar Hydraulic Fractures in Horizontal Wells." Paper IPTC 17043 presented at International Petroleum Technology Conference, Beijing, China, March 26–28, 2013.

Yu, W., and Sepehrnoori, K. "An Efficient Reservoir Simulation Approach to Design and Optimize Unconventional Gas Production." Paper SPE 165343 presented at SPE Western Regional & AAPG Pacific Section Meeting, Monterey, CA, April 19–25, 2013a.

Yu, W., and Sepehrnoori, K. "Simulation of Proppant Distribution Effect on Well Performance in Shale Gas Reservoirs." Paper SPE 167225 presented at SPE Unconventional Resources Conference–Canada, Calgary, Alberta, Canada, November 05-07, 2013b.

Yu, W., and Sepehrnoori, K. "Numerical Evaluation of the Impact of Geomechanics on Well Performance in Shale Gas Reservoirs." Paper ARMA 555 presented at 47th US Rock Mechanics/Geomechanics Symposium, San Francisco, CA, June 23-26, 2013c.

Yu, W., and Sepehrnoori, K. "Simulation of Gas Desorption and Geomechanics Effects for Unconventional Gas Reservoirs." Fuel, 116 (2014): 455–464.

Yu, W., Luo, Z., Javadpour, F., Varavei, A., and Sepehrnoori, K. "Sensitivity Analysis of Hydraulic Fracture Geometry in Shale Gas Reservoirs." Journal of Petroleum Science and Engineering 113 (2014): 1-7.

Wei Yu is a PhD candidate in the Department of Petroleum and Geosystems Engineering at The University of Texas at Austin. His research is focused on optimization of hydraulic-fracture treatments design for shale-gas reservoirs and CO_2 injection for enhanced oil recovery in tight oil reservoirs. He holds a BS degree in applied chemistry from the University of Jinan in China, and an MS degree in chemical engineering from Tsinghua University in China. He is an active member of SPE and the American Association of Petroleum Geologists.

Bo Gao currently works as a Senior Research Engineer in the Upstream Research Company at ExxonMobil. His research interests include improved oil recovery, reservoir properties characterization, routine and special core analysis, novel chemical development, and petrophysics. He has published several technical papers in highly regarded journals and conferences and holds two provisional patents. Gao holds a PhD degree in petroleum engineering from The University of Texas at Austin, and ME and BE degrees in mechanical engineering from Tsinghua University China. He serves as a technical editor for SPE Reservoir Evaluation & Engineering and several other international conferences.

Kamy Sepehrnoori is W.A. "Monty" Moncrief Centennial Chair in the Department of Petroleum and Geosystems Engineering at The University of Texas at Austin. His areas of research include computational methods, reservoir simulation development and application, enhanced-oil-recovery modelling, naturally fractured reservoirs, inverse problems, and unconventional resources. Sepehrnoori holds a PhD degree in petroleum engineering from The University of Texas at Austin.

Studies on the Effect of Surfactants on Rheology of Synthetic Crude

Ravindra Kumar[1], Sambeet Mohapatra[2], Ajay Mandal[3], Tarun Kumar Naiya[4]*

Department of Petroleum Engineering, Indian School of Mines, Dhanbad, 826004, Jharkhand, India

Emails: [1]ravindra01d.kumar@gmail.com; [2]sambeetmech88@gmail.com; [3]ajay_mandal@yahoo.com;
*[4]trn2711@yahoo.com

Abstract

The heavy and extra heavy crude oil from all over the world possess the non-Newtonian flow behavior which results in serious problems related to its transportation from oil fields to refineries. The rheological behaviors of synthetic oil with or without surfactants were studied in the present work. Synthetic oil was prepared by mixing heavy paraffin and mineral oil in different proportions. Anionic surfactant SDS (sodium dodecyl sulfate), cationic surfactant CTAB (hexadecyltrimethyl ammonium bromide) and neutral surfactant Brij S-20 (polyethylene glycol octadecyl ether) were used. Experimental measurements were carried out by physica MC01 Rheometer. Effect of several parameters like shear rate, temperature and addition of mineral oil on viscous behaviors had been studied. US200 software package was used to measure desired parameters. The experimental results showed that viscosity of synthetic oil decreased with increasing temperature by 65.8% when temperature of the mixture of 50% heavy paraffin and 50% mineral oil was increased from 25°C to 50°C at 79.24 s^{-1} shear rate and yield stress of mixture was also reduced. 50%-50% mixture of paraffinic and mineral oil required 5.1 Pa yield stress to flow at 25°C whereas by addition of 0.1%wt/v SDS, CTAB and Brij S-20 required yield stress was reduced by 73.5%, 55.23% and 70% respectively. The rheological behaviors were studied using Power law model, Casson Model and Bingham model and Power law model described the experimental data in best way.

Keywords

Shear Stress; Shear Rate; Viscosity; Synthetic Crude; Surfactant

Introduction

Exploration of crude oil is one of the scenarios changing Endeavour of mankind. The demand for crude oil is increasing rapidly. Crude oil production and its transportation to the processing units are of utmost importance in the petroleum industry [1]. Presently, the main problem in petroleum industries is high viscosity or heavy crude oil. The heavy oil accounts for the large fraction of total world's crude oil production. The towering prices and increasing global demand of oil require efficient techniques for speedy transportation of crude oil. Moreover, due to complex nature of crude oil, there are varieties of difficulties in production, refining and transportation [2]. Different methods are used in order to reduce viscosity of crude oil for pipe line transportation. The various methods include its dilution with lighter crudes, which results in a homogenous mixture of lower viscosities. The system is homogenous solution as both the constituents are of organic origin. Alcohols are also added to reduce the viscosity by dilution. Addition of surfactant reduces the viscosity by reducing the interfacial tension. Heating of pipe lines increases the mobility of its components by increasing their kinetic energies [3].

Traditionally, heating has been used for reducing the viscosity, but it has the disadvantage of significant equipment cost and fuel consumption as well as difficulty in restarting after shutdown [4]. Another problem with heating rises when transporting crude oil is required in colder region, remote region, or underwater transfer. So there is a need to switch between different techniques for efficient transportation of crude oil [5]. Another promising technique is formation of crude oil-water emulsion and then transporting it [6]. The emulsion formed in the beginning needs to be demulsified at the utilization end. The added advantage of surfactant addition is that helps in easy demulsification of the emulsion formed when treated accordingly at the receiving end for further treatment [7].

The frictional pressure drop for turbulent flows past a surface can be reduced by adding small concentrations

of high molecular weight polymer to solvent which leads to the possibility of increased pipeline capacities and faster ships [8]. Drag reduction technique is a flow phenomenon by which small amount additives can greatly reduce turbulent friction factor of solvent [9]. Pour points depressants are also used for easy transportation of heavy crude oil [10]. There are chemicals used to reduce the viscosity of crude oil by changing the structure of paraffin wax crystals. These are polyesters of fatty acids which reduce the pour point by inhibiting the agglomeration of wax crystals [11]. When water along with the highly viscous crude oil flows within the pipelines, the core annular flow configuration takes place, which makes savings in power requirement. A particular flow regime is dependent on the interaction of gravitational, inertial and surface tension forces. Annular flow configuration for particular combinations of the oil and water flow rates is much beneficial for reduction in power requirements [12]. Hasan et al., 2010 [13] studied new technique for viscosity reduction and increased the flow ability of heavier crude oil. Author blended it with lighter crude oil which reduced the viscosity of the crude oil to great extent.

The present work is focused on study of reduction in viscosity of synthetic crude oil at different temperature using different surfactants. Synthetic oil was prepared by different combinations of mineral and heavy paraffinic oil. Mineral oil is mixture of lighter alkane that is produced from a mineral resource. Normally mineral oil is obtained from distillate of crude oil having carbon number from C_{15} to C_{35}. Heavy paraffin is highly purified mixture of saturated liquid hydrocarbon having carbon number in the range of C_{40} to C_{60}. They are used as waxes and components of other products [14]. Composition of mixture is selected so that the properties of synthetic crude are similar to those of real field crude oil of different densities. Viscosity and yield stress were measured before and after addition of mineral oil and surfactants at different temperatures. The results of studies were analyzed to get the best option for the reduction of viscosity as well as yield stress.

Materials and Methods

Material Used

The synthetic oil used in the study was prepared by mixing mineral oil and heavy paraffin in different proportions (Table 1) producing a homogenous solution as both the components are obtained from

TABLE 1 COMPOSITIONS OF THE SYNTHETIC CRUDE OIL PREPARED

Sample number	Mineral oil (%)	Heavy paraffin (%)
01	50	50
02	60	40
03	70	30
04	80	20

Crude oil can't be distinguished using naked eyes. Mineral oil, heavy paraffin and SDS (sodium dodecyl sulfate approximately 99% purity, $C_{12}H_{24}SO_4Na$, MW = 288.38) were procured from Thermo Fisher Scientific India Pvt Ltd, Mumbai. CTAB (hexadecyltrimethyl ammonium bromide approximately 98% purity, $CH_3(CH_2)_{15}N(Br)(CH_3)_3$, MW (364.45)) and Brij S-20 (Polyethylene glycol octadecyl ether approximately 98% purity, $C_{18}H_{37}(OCH_2CH_2)_nOH$, MW= 622) were obtained from Thermo Electron LLR ltd Mumbai and Sigma-Aldrich Chemicals Pvt. Limited, Germany respectively.

Experimental Set-up and Measurement

The synthetic oil was prepared by mixing heavy paraffin and mineral oil. 0.1%wt/v of different surfactant solutions were prepared by dissolving 0.1 g of each surfactant into 100 ml of corresponding synthetic oil. The sample was stirred in a MC-MSC-WH magnetic stirrer at 1500 rpm to make it a homogenous system. It was seen that the CTAB was partially soluble in the mixture, whereas, SDS and Brij S-20 were completely soluble. The temperature of the system was varied from 25°C to 50°C. This was done to enhance the solubility of the surfactant in the synthetic oil. The rheological properties of mixtures of mineral oil and heavy paraffin oil were measured using Physcia MC01 Rheometer. The cone and cylinder sensor attachments were used for determination of viscosity at different temperatures and they were maintained by a water bath. The shear rates were varied from 0.1 s^{-1} to 100 s^{-1} within temperature range 25°C- 50°C. The system generated a graph between shear stress vs. shear rate and viscosity vs. shear rate which was used to predict the effect of temperature and surfactant concentration on reduction of viscosity of synthetic oil. Kruss Esay Dyne Tensiometer was used to study the variation in density and interfacial tension at 30°C.

Results and Discussion

Rheological Study

The rheological behavior of waxy oils was considered to be a crucial parameter in the design of a pipeline,

and fuel cracking units. This behavior was found to be sensitive to shear rate, and temperature [15-16].

Variation in Solubility, Density and Interfacial Tension

Density of the synthetic oil of different composition before and after addition of surfactant was measured at 15°C and results are shown in Table 2.

It was observed that after a long mixing time when the solution containing ionic surfactants was kept for a while, some particles were observed to be suspended into the system; and that neutral surfactant readily gets dissolved into the solution as compared to the other ionic surfactants [17]. Neutral surfactant Brij S-20 was completely soluble in the system.

Surface tension is the property of the system which also helps us to study the interaction between the layers of the fluid. Variation in interfacial tension helps to study the viscosity variation of the fluid. Decrease in surface tension accounts for the reduction in viscosity. As we introduce surfactant into the system, it reduces the interfacial tension of the fluid thereby the viscosity [18]. The results at 30°C are shown in Table 2.

TABLE 2 DENSITY AND SURFACE TENSION VARIATION AT 30°C WITH DIFFERENT COMPOSITION OF SYNTHETIC CRUDE OIL AND SURFACTANTS

Components	Density (g/ml) at 30°C	Surface Tension (mN/m) at 30°C
50% mineral oil+50% heavy paraffin	0.838	30.5
60% mineral oil+40% heavy paraffin	0.835	30.1
70% mineral oil+30% heavy paraffin	0.830	29.9
80% mineral oil+20% heavy paraffin	0.828	29.7
50% mineral oil+50% heavy paraffin+0.1%wt/v SDS	0.840	28.1
50% mineral oil+50% heavy paraffin+0.1%wt/v CTAB	0.839	28.3
50% mineral oil+50% heavy paraffin+0.1%wt/v Brij S-20	0.840	28.8

Modeling Analysis of Rheological Properties

The flow behavior of synthetic oil was studied over wide range of shear rate over a range of temperature 25°C-50°C. Figure 1 shows the thermogram in terms of shear stress and shear rate of 50-50 mixture at different temperature.
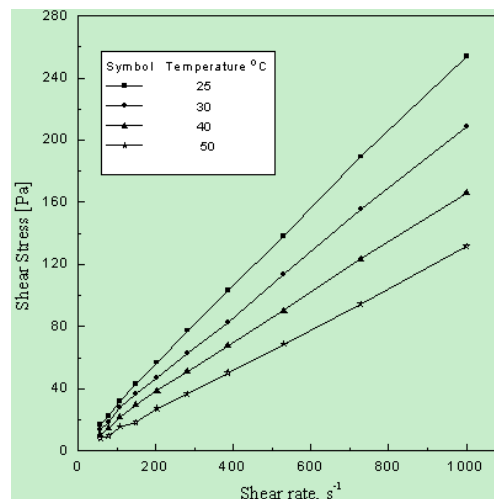

FIG. 1 SHEAR STRESS VS. SHEAR RATE OF 50% MINERAL OIL-50% HEAVY PARAFFIN OIL

Shear stress increased gradually with shear rate. Model analysis was carried out to find certain rheological model that fitted with the experimental data. Three different rheological models namely Power law model [19], Casson model [20], Bingham model [21] as given in Equation 1, 2 and 3 respectively were used to analyze the present data

$$\tau = k\gamma^n \tag{1}$$

$$\tau = \tau_0 + n\gamma \tag{2}$$

$$\tau^{0.5} = \tau_0^{0.5} + (\eta\gamma)^{0.5} \tag{3}$$

Where
τ =applied shear stress (Pa)
γ=shear rate (s^{-1})
k = consistency index (Pa s^n)
n=flow behavior index
τ_0=apparent yield stress (Pa)
η=apparent viscosity (Pa s)

The experimental data were fitted with the above models as shown in Figure 2.
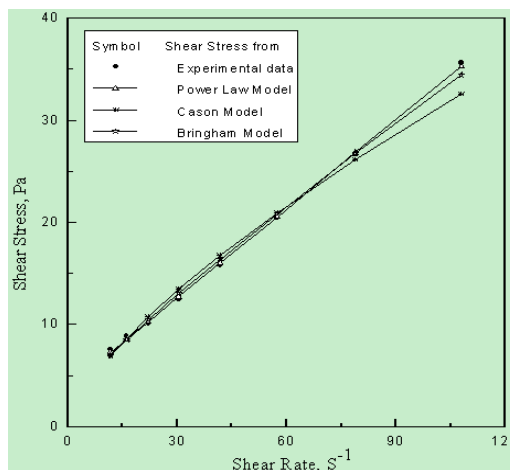

FIG. 2 COMPARISON OF SUGGESTED RHEOLOGICAL MODELS AT 25°C

From the figure, it was concluded that Power law Model was the best model to describe the experimental data over the tested range of shear rate. This was also supported by the data from the Table 3 in which the highest R^2 for power law model was reported.

TABLE 3 MODELING ANALYSIS OF EXPERIMENTAL DATA

Power law model	K =1.234	n = 0.6997	R^2 = 0.9956
Casson model	τ_0 = 3.8613	η = 0.291	R^2 = 0.9912
Bingham model	τ_0 = 1.1253	η = 0.2142	R^2 = 0.9904

The change in rheological properties was modeled and studied using power law model. Pseudo plastic fluid without yield stress obeys the power-law model and that one with yield stress follow Herschel–Buckley model. Bingham plastic and Casson type of fluids are non-Newtonian fluids with yield stress and are called as viscoplastic materials.

Waxy crude oils at low-temperature exhibit viscoplastic behavior [22]. Using power law model [19] the flow behavior index (n) and consistency index (K) were calculated from the following equations and results are shown in Table 4.

$$\log \tau = \log k + n \log \gamma \qquad (4)$$
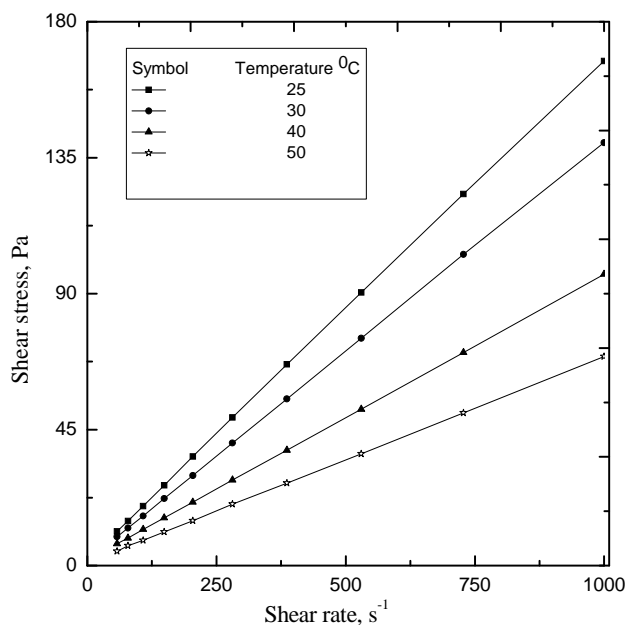
FIG. 3 SHEAR STRESS VS SHEAR RATE 80% MINERAL OIL-20% HEAVY PARAFFIN

TABLE 4 DETERMINATION OF RHEOLOGICAL MODEL PARAMETERS

Temperature (0C)	Composition of mineral oil and heavy paraffinic							
	50-50		60-40		70-30		80-20	
	k	n	k	n	k	n	k	n
25	0.380	0.986	0.342	0.951	0.300	0.955	0.234	0.949
30	0.320	0.945	0.281	0.947	0.253	0.950	0.197	0.947
40	0.250	0.942	0.209	0.928	0.193	0.933	0.170	0.911
50	0.141	0.941	0.176	0.901	0.154	0.914	0.108	0.931

The values of behavior index (n) are less than 1. So it can be concluded that for given compositions at different temperatures the mixture shows pseudo plastic behavior [23].

Effect of Shear Rate on Viscosity at Different Temperature for Synthetic Oil

Effect of shear rate on viscosity at different temperatures was studied and depicted in Figure 4 and Figure 5.
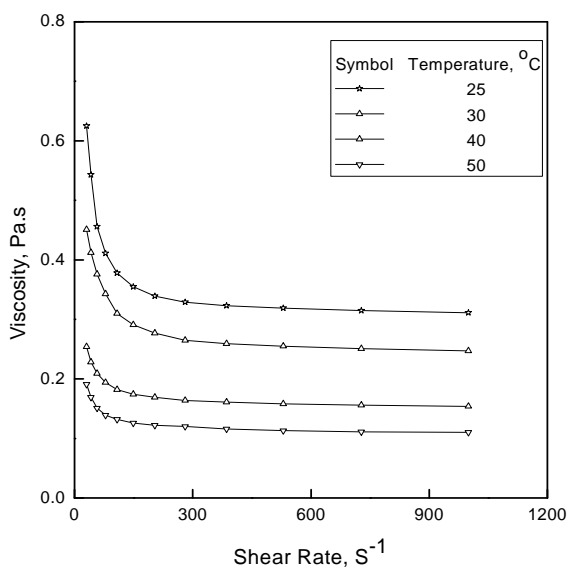

FIG. 4 VISCOSITY VS SHEAR RATE OF 50% MINERAL OIL-50% HEAVY PARAFFIN
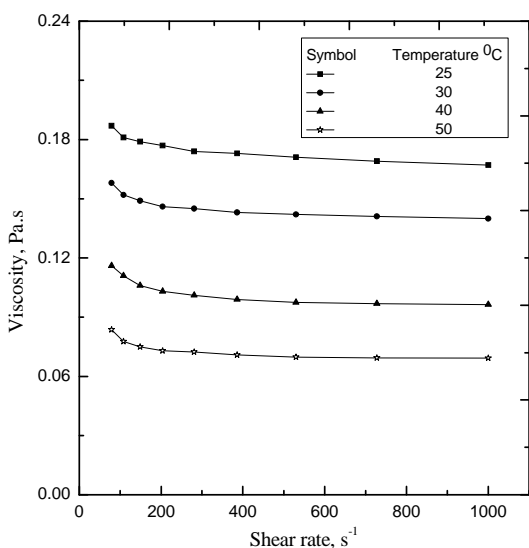

FIG. 5 VISCOSITY VS SHEAR RATE OF 80% MINERAL OIL-20% HEAVY PARAFFIN

Results showed that the shear rate has considerable effect on viscosity particularly at low temperatures. This rheological behavior of the crude may be explained in terms of its composition in the light of the following considerations: At high temperatures synthetic oil behaves like a typical homogeneous isotropic liquid with Newtonian character [24]. Under these circumstances, the viscosity is influenced by two parameters: the effect of temperature reduction that causes increase in viscosity at a particular shear rate. Further cooling causes formation of a gel network leading to progressive rise in viscosity at relatively small dynamic gel strength. On the other hand, the energy exerted by shear is dissipated in the synthetic crude, which leads to disruption of these bonds. This leads to occurrence of accumulated deformation of the crude gel structure [25-26]. As shown in Figure 4 and 5 at lower shear rates, viscosity is higher which becomes constant after the shear rate goes on increasing. This is due to the permanent dissipation of heavier components at higher shear rate.

Yield Stress Measurements

If applied stress is lower than the yield stress then with the release of the applied stress, the sample will regain its original form and will not flow. As the applied stress is increased, yield stress is achieved and permanent deformations will be noted and the sample will start to flow. The yield stress measurements of a sample were carried out at different temperatures employing Physcia MC 01 Rheometer. Relationship between the shear stress and response of shear rate at different temperature for synthetic oil of different composition is shown in Figures 1 and 3. Yield stress was measured from the intercept of the plot. It was observed that the yield stress was required to start the flow decreasing with increase in temperature; as well as that required yield stress of the synthetic oil (50% mineral oil and 50% heavy paraffin) oil was 5.008 Pa and 4.226 Pa at 25°C and 30°C respectively. Again at 50°C, it was reduced to 1.6962 Pa. With the addition of mineral oil (60% mineral-40% heavy paraffin and 70% mineral-30% heavy paraffin) further reduction of yield stress was observed. Table 5 depicted the measured yield stress for synthetic oils of different composition at different temperatures.

It can be concluded that the presence of light oil within the synthetic oil greatly reduces the yield stress which makes the start of flow easier.

TABLE 5 YIELD STRESS MEASUREMENT TEMPERATURE RANGE OF 25°C – 50°C FOR MINERAL OIL OF DIFFERENT COMPOSITION

Composition (% of mineral oil and Heavy Paraffin)	Temperature (°C)	Yield Stress (Pa)	% reduction in yield stress
50-50	25	5.008	0
	30	4.226	15.615
	40	3.884	22.444
	50	1.696	66.134
60-40	25	2.500	50.080
	30	2.135	57.368
	40	2.067	58.726
	50	1.542	69.209
70-30	25	2.257	54.932
	30	2.080	58.466
	40	1.809	63.878
	50	1.482	70.407
80-20	25	2.113	57.808
	30	1.743	65.196
	40	1.533	69.389
	50	1.019	79.652

Effect of Addition of Mineral Oil on Viscosity

The viscosity variation with increasing concentration of mineral oil in the system was studied at different temperatures. This will help us in determining the optimum fluid concentration for fluid pump ability necessary for efficient flow at different conditions of concentrations and temperature. The viscosity of the waxy crudes can be greatly reduced by a continued shear. This fact seems to indicate a kind of "thixotropy." The disintegration of large wax agglomerates appears to be the primary cause for reduction in the viscosity of the system [27].

Figures 4-5 show viscosity variation with shear rate for different composition of synthetic oil. It is evident that as the shear rate increases, the viscosity of the system decreases exponentially within the experimental range of temperature varying from 25°C to 50°C and shear rate varying from 30 s⁻¹ to 1000 s⁻¹. Moreover, the results of viscosity variation are in confluence with the values of behavior index which predicts the pseudo plastic behavior of the system. It was seen from Figures 4-5 that with increasing volumetric concentration of mineral oil in the system, there was

an appreciable decrease in the viscosity of the system. From the above studies, it can be concluded that addition of mineral oil to the system could be a good option for the viscosity reduction of the crude containing heavy paraffin. Viscosity at 79.86 s⁻¹ shear rate in 50-50 vol% and 80-20 vol% mineral oil heavy paraffin were 408 cp and 186 cp respectively, which signifies that the addition of mineral oil is very effective for reduction in viscosity. This large reduction of viscosity with changing shear rate and increasing mineral oil concentration gives us a wide perspective to reduce crude oil viscosity for increasing its flow ability.

It was observed that viscosity shows larger variation at lower shear rates as compared to higher shear rates. With increase in temperature, higher molecular weight components of synthetic oil are not able to agglomerate and form aggregates and hence breaking the bond between the solid particles, which leads to reduction in viscosity. To determine the extent of viscosity reduction, a new parameter DVR (Degree of viscosity reduction) is calculated using the following equations and the results are shown in Table 6.

TABLE 6 DVR% OVER A TEMPERATURE RANGE OF 25°C – 50°C FOR MINERAL OIL OF DIFFERENT COMPOSITION

Composition (% of mineral oil and Heavy Paraffin)	Temperature (°C)	Viscosity (at 79.9 S⁻¹ shear rate)	DVR (%)
50-50	25	0.4082	0
	30	0.3427	16.04
	40	0.1914	53.11
	50	0.1396	65.8
60-40	25	0.2792	31.6
	30	0.2268	44.43
	40	0.1525	62.64
	50	0.1163	71.5
70-30	25	0.2506	38.6
	30	0.205	49.77
	40	0.149	63.49
	50	0.1082	73.49
80-20	25	0.1822	55.36
	30	0.1546	62.12
	40	0.113	72.31
	50	0.0796	80.49

$$DVR\% = \frac{(N_r - N_c)}{N_r} \times 100 \qquad (5)$$

Where, N_r is the reference viscosity at 79.239 s⁻¹ shear rate and 25°C, N_c is the viscosity at 79.239 s⁻¹ shear rate

and corresponding temperature. From the Table 6, it was observed that there is a considerable increase in DVR% from 0% to 65.08% over a temperature range of 25°C – 50°C for 50 vol% mineral oil and 50 vol% heavy paraffin composition. The increase in DVR% can be cited for many reasons. Increase in temperature leads to reduction in the viscosity of the high weight components of synthetic crude oil i.e. waxes and asphaltenes. The other reason is due to effect of temperature which leads to breaking of the ordered structure of higher molecular weight components of synthetic crude oil.

From the Figure 6, it was observed that addition of surfactant greatly reduces the yield stress. Addition of 0.1%wt/v Brij S-20 and 0.1%wt/v CTAB diminishes the yield stress value at 25°C to 54.41% and 69.51% respectively (Table 7).
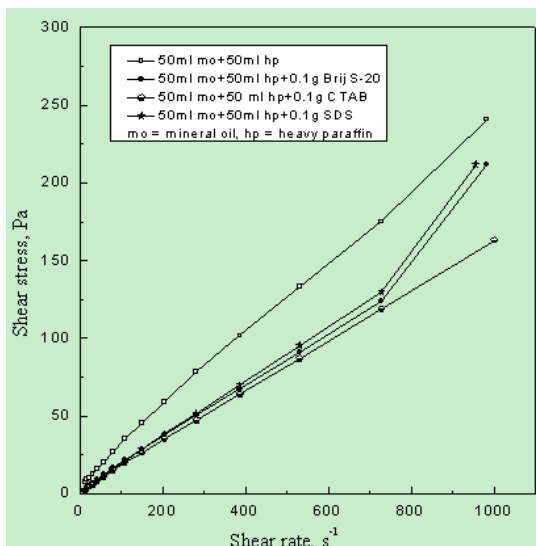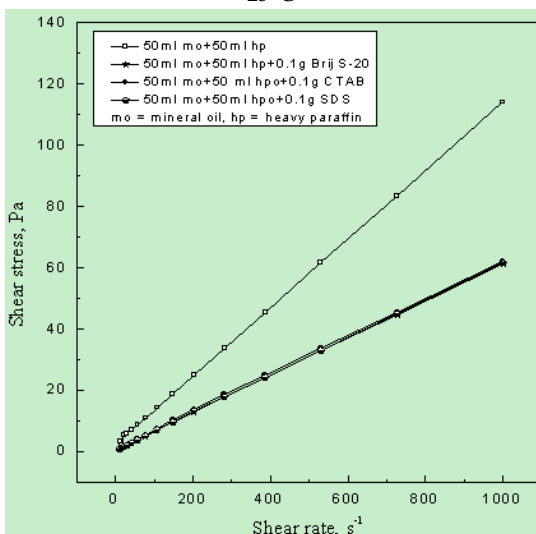
But maximum reduction in yield stress value was observed with the addition of 0.1%wt/v SDS (73.02%) at the corresponding temperature. Addition of surfactant reduces the interfacial tension which was responsible to split the droplets into smaller ones. This helped the synthetic oil easy to flow. At higher temperature, SDS is also the most effective on reduction of yield stress compared to other surfactant.

Effect of Addition of Surfactant on Viscosity

Figure 8 shows the effect of surfactant addition on viscosity at 25°C for 50%-50% mixture. At 78.9 s^{-1} shear rate (25°C), viscosity of the mixture without addition of surfactant was 0.32 Pas whereas with addition of 0.1%wt/v of SDS, CTAB and Brij S-20 the DVR were calculated as 37.2%, 41.6% and 34.5% respectively.

FIG. 6 SHEAR STRESS VS SHEAR RATE FOR DIFFERENT SURFACTANTS AT 25°C

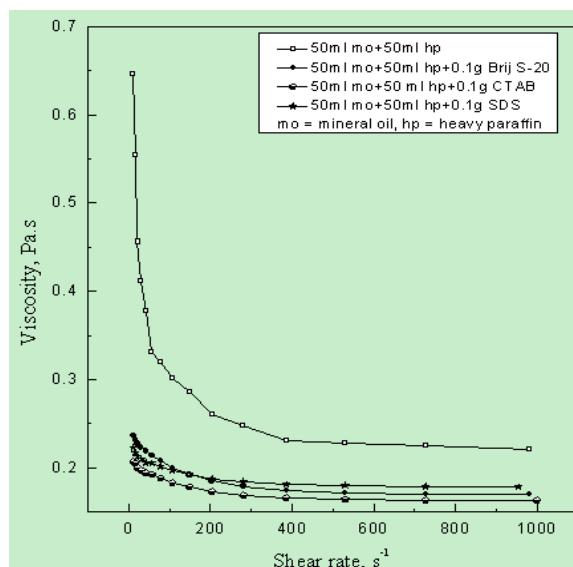FIG. 8 VISCOSITY VS SHEAR RATE FOR DIFFERENT SURFACTANTS AT 25°C

FIG. 7 SHEAR STRESS VS SHEAR RATE FOR DIFFERENT SURFACTANTS AT 50°C
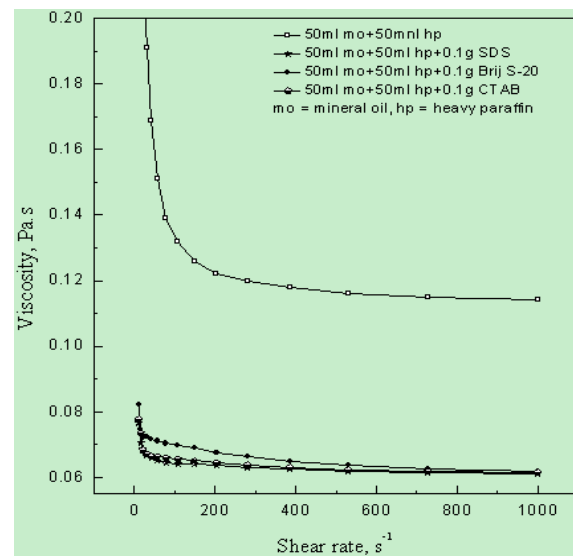

FIG. 9 VISCOSITY VS SHEAR RATE FOR DIFFERENT SURFACTANTS AT 50°C

TABLE 7 EFFECT OF SURFACTANTS ON YIELD STRESS FOR 50-50% SYNTHETIC OIL OVER A TEMPERATURE RANGE OF $25^\circ C - 50^\circ C$

Temp(°c)	Yield stress (pa)				% reduction of yield stress		
	Without surfactant	With surfactant			With surfactant		
		0.1g SDS	0.1g CTAB	0.1g Brij S- 20	0.1g SDS	0.1g CTAB	0.1g Brij S- 20
25	5.008	1.351	1.527	2.283	73.02	69.51	54.41
30	4.226	1.108	2.019	0.957	73.78	52.22	77.35
40	3.884	0.530	0.694	0.982	86.35	82.13	74.76
50	1.696	0.290	0.346	0.642	82.91	79.60	62.15

TABLE 8 DVR% WITH THE ADDITION OF DIFFERENT SURFACTANTS ON SYNTHETIC OIL (50-50% MIXTURE) AT DIFFERENT TEMPERATURE AT $78.9 \, s^{-1}$ SHEAR RATE

Temp(°c)	Viscosity without surfactant (Pa s)	Without surfactant DVR%	With surfactant viscosity (Pa.s)			DVR % with surfactant		
			0.1g SDS	0.1g CTAB	0.1g Brij S-20	0.1g SDS	0.1g CTAB	0.1g Brij S-20
25	0.4082	0	0.201	0.187	0.209	37.2	41.6	34.5
30	0.3427	16.04	0.144	0.1513	0.1642	64.72	62.93	59.77
40	0.1914	53.11	0.0937	0.096	0.0703	77.04	76.48	82.77
50	0.1396	65.8	0.0641	0.0659	0.0402	84.29	83.85	89.25

These surfactants are also effective to reduce the viscosity significantly at higher temperature. Variation of viscosity with shear rate at 50°C with addition of surfactants is shown in Figure 9 and results are depicted in Table 8.

Degree of viscosity reduction increased with increase in temperature from 25°C to 50°C (Table 8) for all of the surfactants used in our study. The highest degree of viscosity reduction (DVR = 41.6) was observed for surfactant CTAB at lower temperature (25°C). At higher temperature (40°C and 50°C) Brij S-20 resulted highest DVR% (82.77% and 89.25%) amongst the three surfactants. This can be explained by the fact that at lower temperature cationic surfactant CTAB is more reactive to heavy paraffin whereas at higher temperature neutral surfactants Brij S-20 become more active to react with heavy paraffin and reduce the viscosity in very great extent.

Conclusion

Effect of mineral oil addition and temperature on viscosity and yield stress of heavy paraffinic oil were studied. Different surfactants like SDS, CTAB and Brij S-20 were also used to reduce the viscosity and minimum stress required to flow of synthetic oil. From the above studies, it can be concluded that

i. Ionic surfactants are partially soluble in the synthetic crude oil whereas neutral surfactants are completely soluble.

ii. Due to addition of mineral oil in the synthetic oil, the viscosity of the mixture was greatly reduced. So mineral oil addition may be one of the alternatives for the reduction of viscosity of crude oil.

iii. Yield stress required to flow also decreased considerably with the addition of mineral oil. So less power will be required for starting of flow if mineral oil is added.

iv. Increase in temperature also had positive effect on the flow ability of synthetic oil as it decreased the viscosity and yield stress. So heating may be the alternative for flow assurance.

v. At lower temperature, CTAB is more effective to reduce the viscosity compared to other surfactants whereas at higher temperature Brij S-20 is the best one. Over the entire range of temperature, maximum reduction in the yield stress was noticed after SDS addition followed by CTAB and Brij S-20. So considering both yield stress and viscosity reduction, SDS seems to be best one.

REFERENCES

[1] Thuc, P. D., Bich., H. V., Son, T. C., Hoe, L. D., Vygovskoy V. P., Vietsovpetro, J. V., "The Problem in Transportation of High Waxy Crude Oils Through Submarine Pipelines at JV Vietsovpetro Oil Fields", Offshore Vietnam" Journal of Canadian Petroleum Technology (2006) Volume 42-6. 15-18.

[2] AI-Besharah, J. M., Salman, O. A., Akashah S. A.,, "Viscosity of crude oil blends. Industrial and Engineering Chemistry Research", 26 (1987): 2445-244.

[3] Al-Roomi,Y., George, R., Elgibaly, A., Elkamel, A., , Use of a novel surfactant for improving the transportability/transportation of heavy/viscous crude oils", Journal of Petroleum Science and Engineering 42 (2004): 235– 243.

[4] Zhang, J., Chen, D., Yan, D., Yang, X., , "Pipelining of Heavy Crude Oil as Oil-in-Water Emulsions", , Society of Petroleum Engineers. (1991) 21733-MS 911-918.

[5] Ghannam, M. T., Hasan, S. W., Abu-Jdayil, B., Esmail, N., ., "Rheological Properties Of Heavy & Light Crude Oil Mixtures For Improving Flowability", Journal Of Petroleum Science And Engineering (2102) 81 122-128.[6]Abdurahman, N. H., Rosli, Y. M., Azhari, N. H., Hayder, B. A., ,"Pipeline transportation of viscous crudes as concentrated oil-in-water emulsions" , Journal of Petroleum Science and Engineering, 90–91 (2012): 139–144.

[6] Farah, M. A., Oliveira, R. C., Caldas, J. N., Rajagopal, K., "Viscosity of water-in-oil emulsions: Variation with temperature and water volume fraction", Journal of Petroleum Science and Engineering (2005) 48 169– 184.

[7] Daas, M., Bleyle, D., "Computational and experimental investigation of the drag reduction and the components of pressure drop in horizontal slug flow using liquids of different viscosities", Experimental Thermal and Fluid Science (2006) 30 307–317.

[8] Mansour, A., Swaiti, O., Aldoss, T., Issa, M., "Drag reduction in turbulent crude oil pipe line using a new chemical solvent", International Journal of Heat and Fluid Flow. 1988 9 316–320.

[9] Deshmukh, S., Bharambe, D. P., "Synthesis of polymeric pour point depressants for Nada crude oil", (Gujarat, India) and its impact on oil rheology, Fuel Processing Technology (2008) 89 227–233.

[10] Soni, H. P., Kiranbala, Bharambe, D. P., , "Performance-based design of wax crystal growth inhibitors", J .Energy Fuels (2008) 22 3930-3938.

[11] Pietro Poesio, P., Strazza, D., Sotgia, G. , "Very-viscous-oil/water/air flow through horizontal   pipes", Chemical Engineering Science (2009) 64 1136-1142.

[12] Hasan, S. W., Ghannam, M. T., Esmail, N., "Heavy Crude Oil Viscosity Reduction and Rheology Pipeline Transportation", Fuel (2010) 89 1095-1100.

[13] EFSA., "Scientific Opinion on Mineral Oil Hydrocarbons in Food", EFSA Journal (2012) 10(6):2704

[14] Halim, N., Ali, S., Nadeem, M., Hamid, P. A., Tan, I. M., , "Synthesis of Wax Inhibitor and Assessment of Squeeze Technique Application for Malaysian Waxy Crude", SPE (2011) 20-22.

[15] Meriem-Benziane, M., Abdul-Wahab, S. A., Benaicha, M., Belhadri, M.,   "Investigating the rheological properties of light crude oil and the characteristics of its emulsions in order to improve pipeline flow", Fuel (2012) 95 97–107.

[16] Neogi, P., Munden, J. J., "Solubilization kinetics of soluble oils by an ionic surfactant", Journal of Colloid and Interface Science (2007) 305 202–203.

[17] Pekdemir, T., Çopur, M., Urum, K., , "Emulsification of Crude Oil–Water Systems Using Bio surfactants", Process Safety and Environmental Protection (2005) 83(B1): 38–46.

[18] De Waele, A. "Viscometry and Plastometry", Journal of the Oil & Colour Chemists Association 6 (1923) 33–69.

[19] Casson, N., "A flow equation for pigment–oil suspensions of the printing ink type. In C. C. Mill (Ed.)" Rheology of disperses suspensions, (1959): 84–104.

[20] Bingham, E. C., "Fluidicv and Plasticity, McGraw-Hill Book Co. Inc., New York (1922).

[21] Martínez-Palou, R., Mosqueira, M. de L., Zapata-Rendón, Beatriz, Mar-Juárez, E., Bernal-Huicochea, C., Clavel-López, J. de la C., Aburto, J., , "Transportation of heavy and extra-heavy crude oil by pipeline: A review", Journal of Petroleum Science and Engineering (2011) 75 274–282.

[22] Caenn, R., Darley, H. C. H., Gray G. R., "Composition and Properties of Drilling and Completion Fluids", Elsevier 2011, 197-235.

[23] Al-Zahrani, S. M., Al-Fariss, T. F., "A general model for the viscosity of waxy oils", Chemical Engineering and Processing (1998): 37 433–437.

[24] Taraneh, J. B., Rahmatollah, G., Hassan, A., Hassan, A.,, "Effects of wax inhibitors on pour point and rheological properties of Iranian waxy crude oil" , Fuel Processing Technology (2008) 89 973–977.

[25] Fasslhl, M. R., Meyers, K. O., Welsbrod, K. R., , "Thermal Alteration of Viscous Crude Oils", 14225-PA, SPE Reservoir Engineering Volume (1990) 5-3 393-401.

[26] Farina, A., Fasano, A., "Flow Characteristics of Waxy Crude Oils in Laboratory Experimental Loops", Mathl. Comput. Modelling Vol. 25, No. 5, pp. (1997) 75-86.

BIOGRAPHIES

Ravindra Kumar, born in 1986 in Jharkhand, India is currently pursuing Ph.D. from Department of Petroleum Engineering, Indian School of Mines, Dhanbad, under the guidance of Dr. T. K. Naiya and Dr. A. Mandal. He completed his graduation in Chemical engineering in 2011. Research interest is on study on multiphase flow of oil water and gas in horizontal and vertical pipes.

Sambeet Mohapatra, born in 1988 in Odisha, India is currently pursuing M.Techfrom Department of Petroleum Engineering, Indian School of Mines, Dhanbad, under the guidance of Dr. T.K. Naiya. He completed his graduation in Mechanical Engineering in 2012.

Dr. A. Mandal is Associate Professor in Department of Petroleum Engineering, Indian School of Mines, Dhanbad. He has done B.Sc. (Chemistry Hons.) from Calcutta University, B.Tech. in Chemical Engineering Calcutta University, M.ChE. in Chemical Engineering Jadavpur University, Ph.D. in Chemical Engineering IIT, Kharagpur. Specializes in Natural Gas Engineering, Thermodynamics of Res. Fluids, EOR Techniques, Oil and Gas Plant Design. Research interest: Fluid Mechanics and Multiphase Flow, EOR Techniques, Gas Hydrates, Separation of oil from oil-in–water Emulsion.

Dr. T. K. Naiya is Assistant Professor in Department of Petroleum Engineering, Indian School of Mines, Dhanbad. He has Ph. D. in Chemical Engineering, M. Tech. in Chemical Engineering, B. Tech. in Chemical Engineering, Specializes in Petroleum and Petrochemical Refinery Engineering, Reactor design, Fluid Mechanics, Environmental Engineering, Process heat transfer. Research interest is Waste water management, Adsorption, Membrane Separation, Non-conventional energy sources, Chemical Reaction Engineering.